

Electronic ISSN: 1309-0267



**International Journal  
of Engineering &  
Applied Sciences**

**I  
J  
E  
A  
S**

**IJEAS**

**Volume 15, Issue 2  
2023**

Published by Akdeniz University

## **HONORARY EDITORS**

*(in alphabetical order)*

- Prof. Atluri, S.N.- University of California, Irvine-USA  
Prof. Liew, K.M.- City University of Hong Kong-HONG KONG  
Prof. Lim, C.W.- City University of Hong Kong-HONG KONG  
Prof. Liu, G.R.- National University of Singapore- SINGAPORE  
Prof. Nath, Y.- Indian Institute of Technology, INDIA  
Prof. Omurtag, M.H. -ITU  
Prof. Reddy, J.N.-Texas A& M University, USA  
Prof. Saka, M.P.- University of Bahrain-BAHRAIN  
Prof. Shen, H.S.- Shanghai Jiao Tong University, CHINA  
Prof. Xiang, Y.- University of Western Sydney-AUSTRALIA  
Prof. Wang, C.M.- National University of Singapore- SINGAPORE  
Prof. Wei, G.W.- Michigan State University-USA

## **EDITOR IN CHIEF:**

Assoc. Prof. Ibrahim AYDOGDU -Akdeniz University *aydogdu@akdeniz.edu.tr*

## **ASSOCIATE EDITORS:**

Assist. Prof. Kadir MERCAN –Mehmet Akif Ersoy  
University *kmercan@mehmetakif.edu.tr*

## **SECTION EDITORS:**

- Assoc. Prof. Metin Mutlu Aydın – Ondokuz Mayıs University  
Assoc. Prof. Mustafa Arda –Trakya University  
Assist. Prof. Refik Burak Taymuş- Van 100. Yıl University

## EDITORIAL BOARD

*(The name listed below is not Alphabetical or any title scale)*

Prof. Xinwei Wang -Nanjing University of Aeronautics and Astronautics

Asst. Prof. Francesco Tornabene -University of Bologna

Asst. Prof. Nicholas Fantuzzi -University of Bologna

Assoc. Prof. Keivan Kiani - K.N. Toosi University of Technology

Asst. Prof. Michele Baccocchi -University of Bologna

Asst. Prof. Hamid M. Sedighi -Shahid Chamran University of Ahvaz

Prof. Yaghoub Tadi Beni -Shahrekord University

Prof. Raffaele Barretta -University of Naples Federico II

Prof. Meltem ASİLTÜRK -Akdeniz University *meltemasilturk@akdeniz.edu.tr*

Prof. Metin AYDOĞDU -Trakya University *metina@trakya.edu.tr*

Prof. Ayşe DALOĞLU - KTU *aysed@ktu.edu.tr*

Prof. Oğuzhan HASANÇEBİ - METU *oguzhan@metu.edu.tr*

Asst. Prof. Rana MUKHERJİ - The ICFAI University

Assoc. Prof. Baki ÖZTÜRK - Hacettepe University

Assoc. Prof. Yılmaz AKSU -Akdeniz University

Assoc. Prof. Hakan ERSOY- Akdeniz University

Assoc. Prof. Mustafa Özgür YAYLI -Uludağ University

Assoc. Prof. Selim L. SANİN - Hacettepe University

Asst. Prof. Engin EMSEN -Akdeniz University

Prof. Serkan DAĞ - METU

Prof. Ekrem TÜFEKÇİ - İTÜ

## ABSTRACTING & INDEXING



IJEAS provides unique DOI link to every paper published.

### EDITORIAL SCOPE

The journal presents its readers with broad coverage across some branches of engineering and science of the latest development and application of new solution algorithms, artificial intelligent techniques innovative numerical methods and/or solution techniques directed at the utilization of computational methods in solid and nano-scaled mechanics.

International Journal of Engineering & Applied Sciences (IJEAS) is an Open Access Journal

International Journal of Engineering & Applied Sciences (IJEAS) publish original contributions on the following topics:

**Civil Engineering:** numerical modelling of structures, seismic evaluation, experimental testing, construction and management, geotechnical engineering, water resources management, groundwater modelling, coastal zone modelling, offshore structures, water processes, desalination, waste-water treatment, pavement and maintenance, transport and traffic, laser scanning, and hydrographic surveying, numerical methods in solid mechanics, nanomechanic and applications, microelectromechanical systems (MEMS), vibration problems in engineering, higher order elasticity (strain gradient, couple stress, surface elasticity, nonlocal elasticity)

**Electrical Engineering:** artificial and machine intelligence and robotics, automatic control, bioinformatics and biomedical engineering, communications, computer engineering and networks, systems security and data encryption, electric power engineering and drives, embedded systems, Internet of Things (IoT), microwaves and optics.

**Engineering Mathematics and Physics:** computational and stochastic methods, optimization, nonlinear dynamics, modelling and simulation, computer science, solid state physics and electronics, computational electromagnetics, biophysics, atomic and molecular physics, thermodynamics, geophysical fluid dynamics, wave mechanics, and solid mechanics.

**Mechanical Engineering:** machine design, materials science, mechanics of materials, manufacturing engineering and technology, dynamics, robotics, control, industrial engineering, ergonomics, energy, combustion, heat transfer, fluids mechanics, thermodynamics, turbo machinery, aerospace research, aerodynamics, and propulsion.

IJEAS allows readers to read, download, copy, distribute, print, search, or link to the full texts of articles.



# CONTENTS

**Generalized Programming Idea for Making the Thermoelectric Device Using MATLAB Software for  
Cu<sub>2</sub>Bi<sub>2</sub>Te<sub>3</sub> and Cu<sub>2</sub>Sb<sub>2</sub>Te<sub>3</sub>**

*By Udhaya Sankar Ganesamoorthy*..... 52-59

**Time-Dependent Reliability Analysis for Deflection of a Reinforced Concrete Box Girder Bridge**

*By Abrham Gebre Tarekegn* ..... 60-74

**A Simple Inspection of Arches, Curved Beams, and Shells**

*By Mustafa Şeker Ömer Civalak* ..... 75-85



## Generalized Programming Idea for Making the Thermoelectric Device Using MATLAB Software for $\text{Cu}_2\text{Bi}_2\text{Te}_3$ and $\text{Cu}_2\text{Sb}_2\text{Te}_3$

Udhaya Sankar Ganesamoorthy

National Small Industries Corporation, Chennai – 600032, Tamilnadu, India.

✉: [udhayasankar20@outlook.com](mailto:udhayasankar20@outlook.com), : 0000-0002-1416-9590

Received: 07.03.2023, Revised: 21.04.2023, Accepted: 22.05.2023

### Abstract

Device fabrication using simulation process and modeling are one of the most leading researches in present days. Here, the Thermoelectric Device performance is analyzed with basic coding using MATLAB software. The MATLAB based fabrication of thermoelectric generator lead to analysis the power efficiency and ZT performance for the materials ( $\text{Cu}_2\text{Bi}_2\text{Te}_3$  and  $\text{Cu}_2\text{Sb}_2\text{Te}_3$ ). All parameters were optimized and the function output (Figure of Merit) was 2.59 (no unit) for  $\text{Cu}_2\text{Bi}_2\text{Te}_3$  and 0.657 (no unit) for  $\text{Cu}_2\text{Sb}_2\text{Te}_3$ .

**Keywords:** Thermoelectric Generator; MATLAB device manufacture; Device Performance Analysis, Device fabrication using MATLAB Programming; Thermoelectric Device.

### 1. Introduction

MATLAB provides a potent tool for modeling and analyzing sustainable energy systems, including thermoelectric energy conversion. Its flexibility and versatility, along with its built-in tools and features for numerical analysis and simulation, make it a useful platform for academics and engineers working in the field of sustainable energy [2, 5, 10-12]. For investigating the behavior of thermoelectric materials and devices, MATLAB is an effective tool because to its strengths in numerical methods, data processing, and visualization [6-9]. Optimization of the design and functionality of thermoelectric materials and devices is one potential application of MATLAB in sustainable energy modeling.

The performance of various thermoelectric device designs, such as thermoelectric generators and coolers, under various operating conditions can be simulated using the MATLAB model [3]. The device's efficiency, power output, and cooling capacity can all be predicted using the model, which may also be used to optimize the device's overall design. One of the advantages of the MATLAB model is its simplicity in including user-defined equations and functions, which enables researchers to adapt the model to their particular requirements [3]. Researchers with no programming experience can utilize the Simulink model since it has an intuitive user interface [4]. The simulation's material properties and boundary conditions must be accurate in order for the model to be accurate. Thus, it's crucial to carefully describe for the present thermoelectric generator work. The recent work p-type segment leg resulting  $\text{Sb}_{1.82}\text{In}_{0.15}\text{Cu}_{0.03}\text{Te}_{2.98}$  sample had a ZT value of 1.06 at 623 K and a high ZT of 0.76 from 300 K to 673 K [17]. By manipulating electron & phonon transports, the  $\text{Sb}_2\text{Te}_3(\text{SnMn}_{0.08}\text{Te})_{10}$  achieved a peak ZT of approximately 1.3 at 773 K and an average ZT of around 0.78 between 300 and 823 K [18]. The FOM(ZT) of  $\text{Bi}_2\text{Te}_3$  exhibited a peak value of 1.30 at 450 K and an average ZT of 1.14 between 300 and 500 K [19]. The present work deals with material  $\text{Cu}_2\text{Bi}_2\text{Te}_3$  and  $\text{Cu}_2\text{Sb}_2\text{Te}_3$  for analyzing the Z-T-efficiency.



## 2. Method to create thermoelectric device

Thermoelectric generators (TEGs) are devices that can convert temperature differences into electrical energy using the Seebeck effect. MATLAB software can be used to model and simulate the behavior of TEGs. Here is a way to create a TEG model in MATLAB:

Step 1: Define the material properties of the TEG:

```
alpha = 0.01; % Seebeck coefficient in V/K
k = 2; % Thermal conductivity in W/mK
sigma = 1; % Electrical conductivity in S/m
T_hot = 1000; % Hot side temperature in K
T_cold = 300; % Cold side temperature in K
```

Step 2: Define the geometry of the TEG:

```
length = 0.01; % Length of the TEG in meters
area = 0.001; % Cross-sectional area of the TEG in square meters
```

Step 3: Calculate the voltage and power output of the TEG:

```
deltaT = T_hot - T_cold;
voltage = alpha * deltaT;
power = voltage^2 / (4 * length * (k / area) + (1 / sigma) * length * area);
```

Step 4: Plot the power output as a function of the hot side temperature:

```
T_hot_range = 300:10:1000; % Range of hot side temperatures to test
power_output = zeros(size(T_hot_range));
for i = 1:length(T_hot_range)
    T_hot = T_hot_range(i);
    deltaT = T_hot - T_cold;
    voltage = alpha * deltaT;
    power_output(i) = voltage^2 / (4 * length * (k / area) + (1 / sigma) * length * area);
end
plot(T_hot_range, power_output)
xlabel('Hot side temperature (K)')
ylabel('Power output (W)')
```

This code calculates the power output of the TEG for a range of hot side temperatures and plots the results. You can modify the material properties and geometry of the TEG to simulate different designs and optimize their performance.

## 3. Result and Discussion

The result and discussion of a thermoelectric generator simulation using MATLAB software will depend on the specific model and parameters used. However, here the fig.1 and fig.4 shows the efficiency vs.  $Z$  graph; then fig.2 and fig.5 shows the efficiency vs.  $K$  and the fig.3 and fig.6 shows the  $ZT$ . The output power of a thermoelectric generator depends on the temperature difference between the hot and cold sides of the device. As the temperature

difference increases, so does the power output. The voltage output of the generator is also directly proportional to the temperature difference. The  $\text{Cu}_2\text{Bi}_2\text{Te}_3$  and  $\text{Cu}_2\text{Sb}_2\text{Te}_3$  material properties of the thermoelectric generator should optimize for its performance. By changing the dimensions and materials of the generator, it is possible to enhance its efficiency and Z-T output.

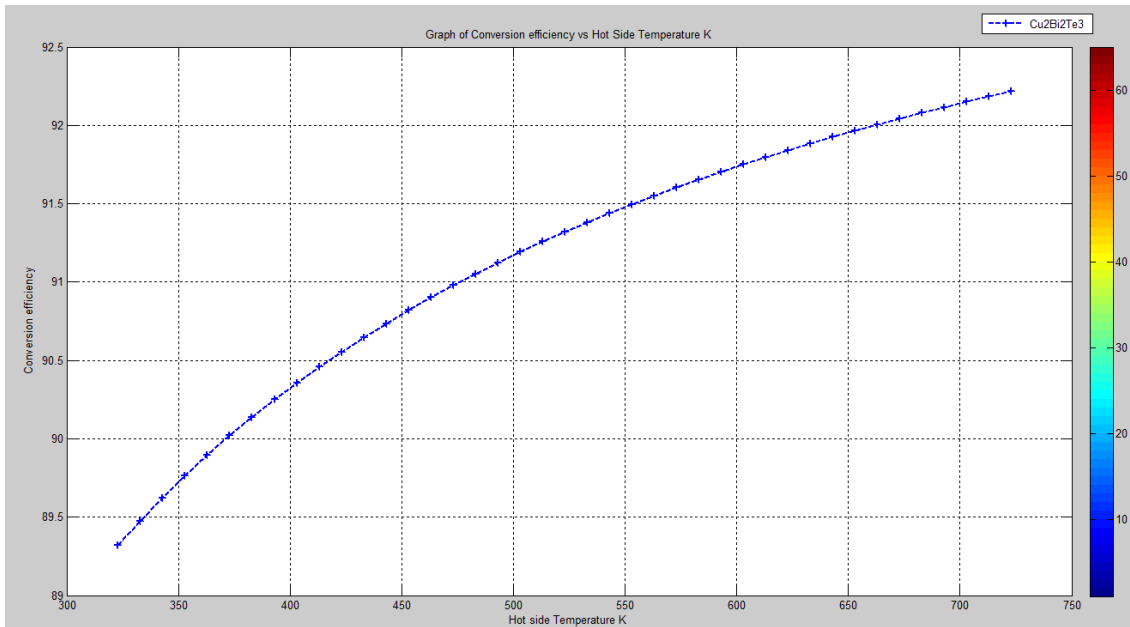


Fig. 1. Efficiency vs Z of  $\text{Cu}_2\text{Bi}_2\text{Te}_3$

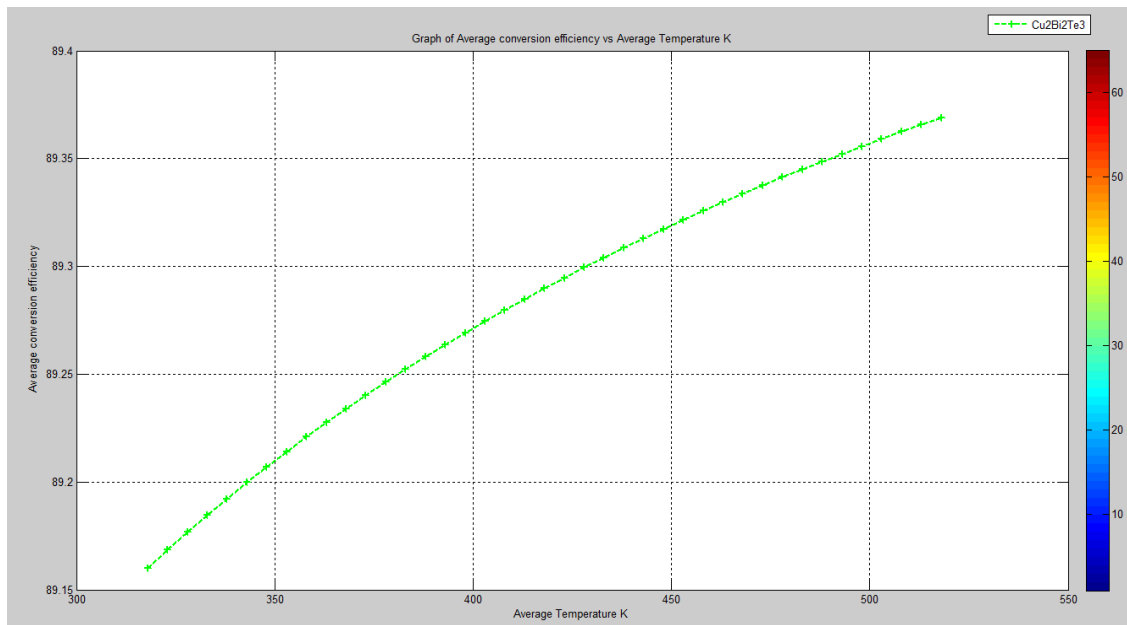


Fig. 2. Efficiency vs K of  $\text{Cu}_2\text{Bi}_2\text{Te}_3$

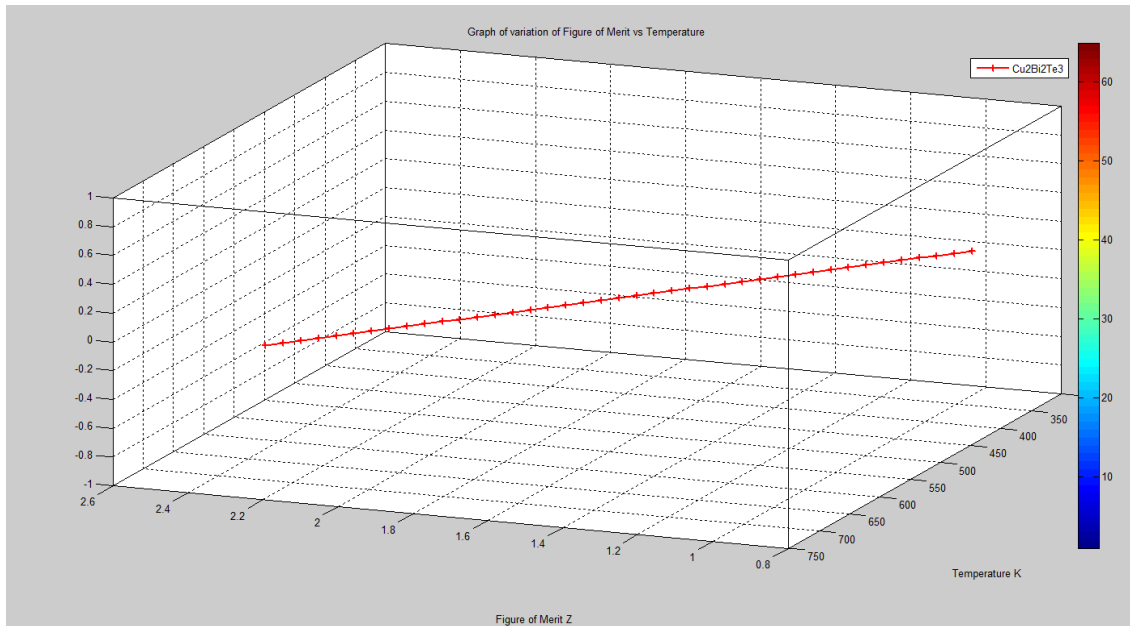


Fig. 3. ZT of  $\text{Cu}_2\text{Bi}_2\text{Te}_3$

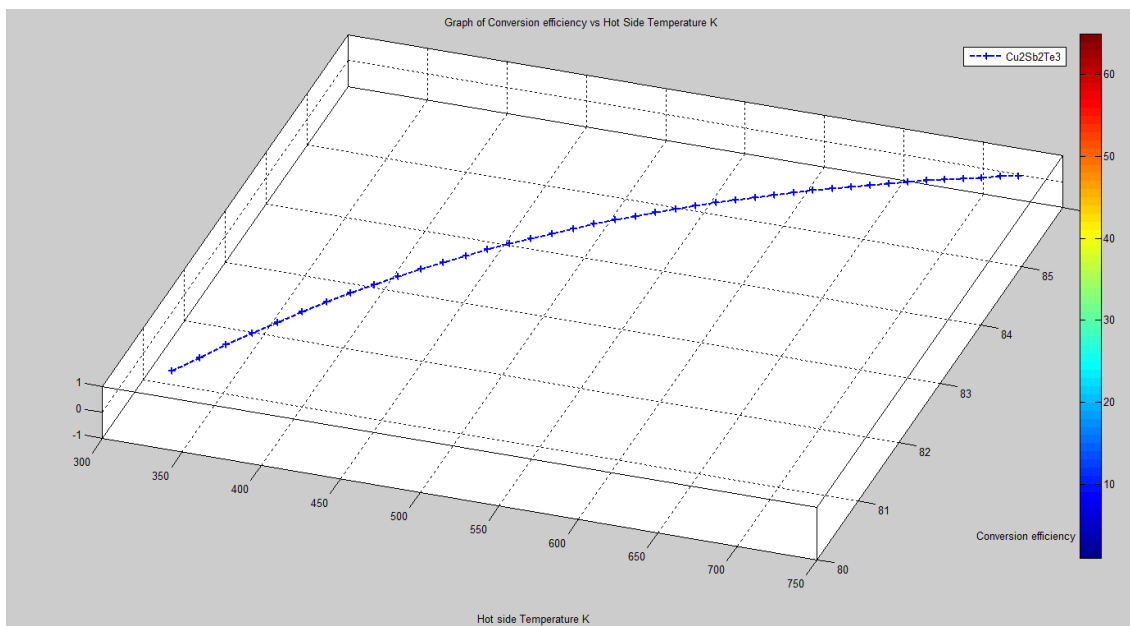


Fig. 4. Efficiency vs Z of  $\text{Cu}_2\text{Sb}_2\text{Te}_3$

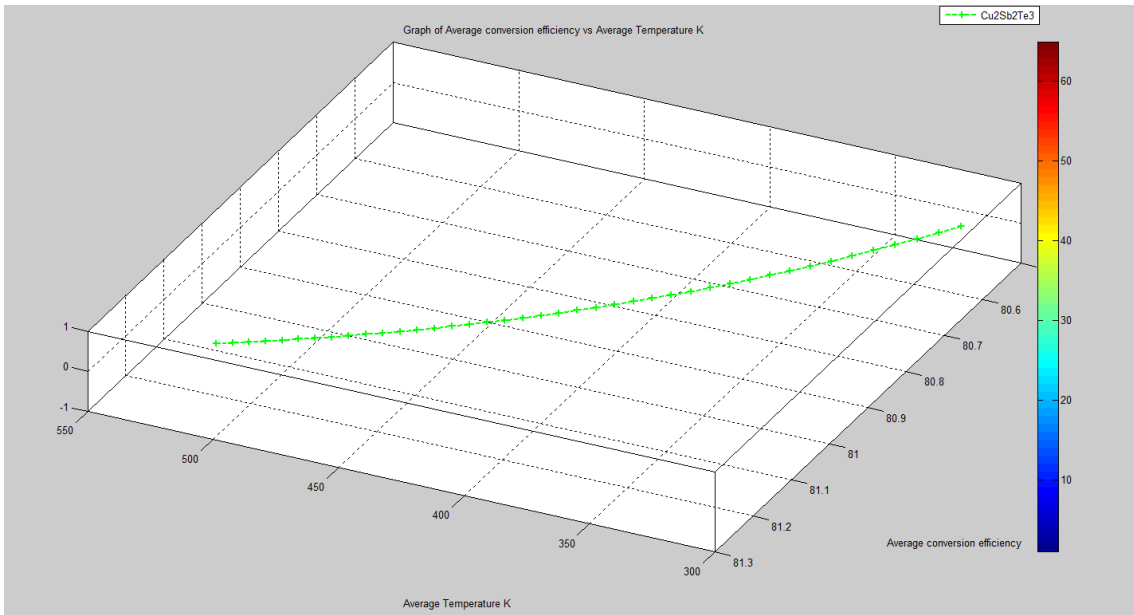


Fig. 5. Efficiency vs K of Cu<sub>2</sub>Sb<sub>2</sub>Te<sub>3</sub>

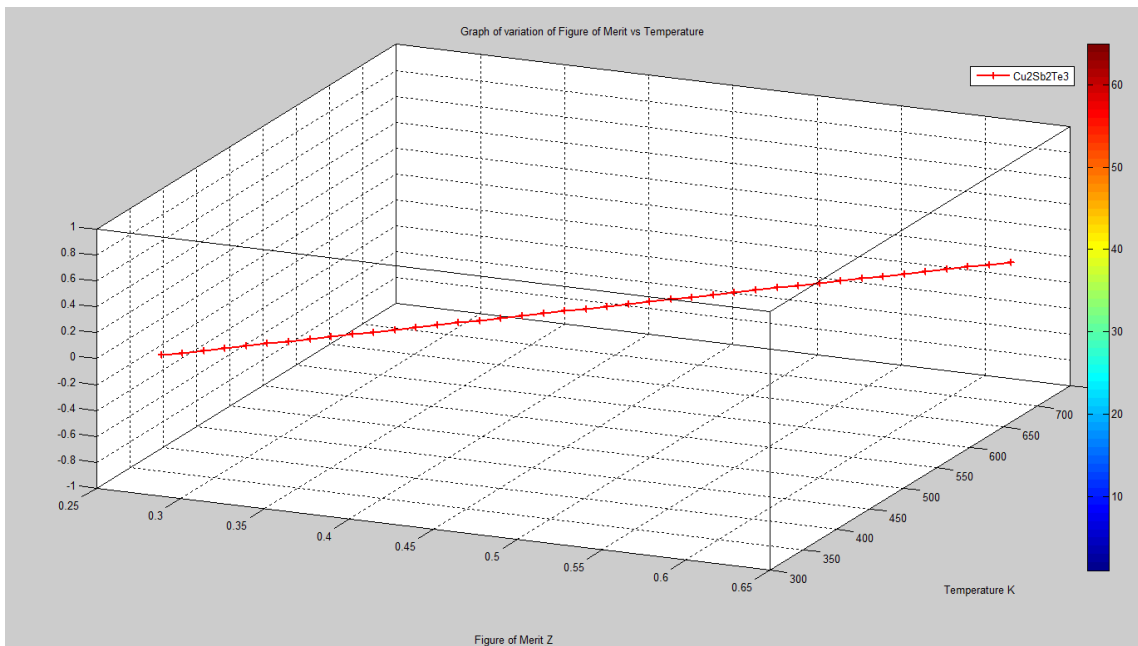


Fig. 6. ZT of Cu<sub>2</sub>Sb<sub>2</sub>Te<sub>3</sub>

One important consideration when designing a thermoelectric generator is the tradeoff between efficiency and power output. Increasing the efficiency of the generator often comes at the cost of reducing its power output, and vice versa. Therefore, designers must carefully balance these factors to achieve the desired performance. Here, Table 1 shows the results of Cu<sub>2</sub>Bi<sub>2</sub>Te<sub>3</sub> and Cu<sub>2</sub>Sb<sub>2</sub>Te<sub>3</sub> Thermoelectric Generator Device and it was compared with Bi<sub>2</sub>Te<sub>3</sub> and Sb<sub>2</sub>Te<sub>3</sub> materials. Cu<sub>2</sub>Bi<sub>2</sub>Te<sub>3</sub> has a higher energy capacity (CC) of 122.4 compared to Cu<sub>2</sub>Sb<sub>2</sub>Te<sub>3</sub>, which has a CC of 98.75. However, Cu<sub>2</sub>Sb<sub>2</sub>Te<sub>3</sub> has a higher density of 2.154 Kg/m<sup>3</sup>, whereas Cu<sub>2</sub>Bi<sub>2</sub>Te<sub>3</sub> has a lower density of 1.156 Kg/m<sup>3</sup>.

Cu<sub>2</sub>Sb<sub>2</sub>Te<sub>3</sub> also has a higher SFC of 264 gm/K-1W-1hr compared to Cu<sub>2</sub>Bi<sub>2</sub>Te<sub>3</sub>, which has an SFC of 224. In terms of power, Cu<sub>2</sub>Bi<sub>2</sub>Te<sub>3</sub> has a higher value of 6.61 kW compared to Cu<sub>2</sub>Sb<sub>2</sub>Te<sub>3</sub>, which has a power value of 4.51 kW. However, Cu<sub>2</sub>Bi<sub>2</sub>Te<sub>3</sub> has a slightly lower volumetric efficiency of 97 compared to Cu<sub>2</sub>Sb<sub>2</sub>Te<sub>3</sub>, which has a volumetric efficiency of 91. The specific heat capacity (Cp) of Cu<sub>2</sub>Bi<sub>2</sub>Te<sub>3</sub> is slightly higher at 1.12 KJ/Kg-1K compared to Cu<sub>2</sub>Sb<sub>2</sub>Te<sub>3</sub>, which has a Cp of 1.09 KJ/Kg-1K. Both materials have the same high and low temperature limits of 725 K and 325 K. Thus, MATLAB software can be used to simulate the behavior of a thermoelectric generator and investigate the effect of various design parameters [1, 3, 4]. This can help researchers and engineers optimize the performance of their devices before building physical prototypes. Overall, the use of MATLAB software for thermoelectric generator design and analysis can lead to more efficient and effective devices with higher power output. The current result of Figure of Merit is 2.59 (no unit) for Cu<sub>2</sub>Bi<sub>2</sub>Te<sub>3</sub> material. The Figure of Merit for Cu<sub>2</sub>Sb<sub>2</sub>Te<sub>3</sub> material is 0.657 (no unit).

Table 1. Thermoelectric Generator Results

<i>Parameter</i>	<i>Material</i>		<i>Comparative results</i>	
	<b>Cu<sub>2</sub>Bi<sub>2</sub>Te<sub>3</sub></b>	<b>Cu<sub>2</sub>Sb<sub>2</sub>Te<sub>3</sub></b>	<b>Bi<sub>2</sub>Te<sub>3</sub></b>	<b>Sb<sub>2</sub>Te<sub>3</sub></b>
Energy capacity (CC)	122.4	98.75	117.5 [13]	100.85 [15]
Density (Kg/m <sup>3</sup> )	1.156	2.154	0.923 [14]	1.953 [16]
SFC (gm/K-1W <sup>-1</sup> hr)	224	264	188 [13]	253 [16]
Power (kW)	6.61	4.51	4.54 [14]	4.39 [15]
Volumetric Efficiency	97	91	117 [14]	99 [15]
Cp (KJ/Kg <sup>-1</sup> K)	1.12	1.09	0.925 [14]	0.863 [16]
High Temperature (K)	725	725	random	random
Low Temperature (K)	325	325	random	random

#### 4. Conclusions

MATLAB software can be a useful tool for designing and analyzing thermoelectric generators. By using MATLAB to simulate the behavior of a TEG, researchers and engineers can investigate the effects of various design parameters, such as the dimensions and material properties of the device, and optimize its efficiency and power output. MATLAB's flexibility and extensive library of functions and tools make it well-suited for modeling and simulating complex systems like TEGs. With MATLAB, it is possible to create detailed and accurate models of TEGs and investigate their performance of Cu<sub>2</sub>Bi<sub>2</sub>Te<sub>3</sub> and Cu<sub>2</sub>Sb<sub>2</sub>Te<sub>3</sub>. In addition to its usefulness in TEG design and analysis, MATLAB can also be used to control and monitor TEGs in real-time, allowing for more precise and efficient operation of these devices. Overall, the use of MATLAB software in thermoelectric generator research and development can lead to more efficient and effective TEGs with higher power output, ultimately contributing to the development of more sustainable and renewable energy systems.

## Acknowledgments

The author likes to thank the reviewers, editors and editor in chief for enrichment of the article by their suggestions.

## References

- [1] Tsai, Huan-Liang, and Jium-Ming Lin, Model building and simulation of thermoelectric module using Matlab/Simulink. *Journal of Electronic Materials*, 39, 5-21, 2010.
- [2] Moorthy, C. Ganesa, and G. Udhaya Sankar, Planck's Constant and Equation for Magnetic Field Waves. *Natural and Engineering Sciences* 4, 107-113, 2019.
- [3] Sankar, G. Udhaya, Ganesa Moorthy, and C. T. Ramasamy, A review on recent opportunities in MATLAB software based modelling for thermoelectric applications. *International Journal of Energy Applications and Technologies* 8, 70-79, 2021.
- [4] Nadimuthu, Lalith Pankaj Raj, Divya Arputham Selvaraj, and Kirubakaran Victor, Simulation and experimental study on performance analysis of solar photovoltaic integrated thermoelectric cooler using MATLAB Simulink. *Thermal Science* 26, 999-1007, 2022.
- [5] Sankar, G. Udhaya, and C. Ganesa Moorthy, Network Modelling on Tropical Diseases vs. Climate Change. *Climate Change and Anthropogenic Impacts on Health in Tropical and Subtropical Regions*. IGI Global, 64-92, 2020.
- [6] Sankar, G. Udhaya, et al. Preparation of CuO<sub>1-x</sub>Mn<sub>x</sub> (x= 0.03, 0.05, 0.07) and MATLAB modelling for sustainable energy harvesting applications. *Journal of Physics: Conference Series*. 1850, 2021.
- [7] Sankar, G. Udhaya, and C. Ganesa Moorthy. *Les mathématiques dans la science des matériaux: pour les études en classe*. Éditions universitaires européennes, 2020.
- [8] Udhaya Sankar, G., C. Ganesa Moorthy, and C. T. Ramasamy, Mathematical Analysis on Power Generation—Part I. *Artificial Intelligence for Renewable Energy and Climate Change* 53-86, 2022.
- [9] Udhaya Sankar, G., C. Ganesa Moorthy, and C. T. Ramasamy, Mathematical Analysis on Power Generation—Part II. *Artificial Intelligence for Renewable Energy and Climate Change* 87-115, 2022.
- [10] Udhaya Sankar, G., C. Ganesa Moorthy, and G. RajKumar. Smart storage systems for electric vehicles—a review. *Smart Science* 7, 1-15, 2019.
- [11] Udhaya Sankar, G. Sustainable Energy Materials. *Artificial Intelligence for Renewable Energy and Climate Change* 117-136, 2022.
- [12] Udhaya Sankar, G., C. Ganesa Moorthy, and G. RajKumar, Synthesizing graphene from waste mosquito repellent graphite rod by using electrochemical exfoliation for

- battery/supercapacitor applications. *Energy Sources, Part A: Recovery, Utilization, and Environmental Effects* 40, 1209-1214, 2018.
- [13] Pei, Jun, Bowen Cai, Hua-Lu Zhuang, and Jing-Feng Li. Bi<sub>2</sub>Te<sub>3</sub>-based applied thermoelectric materials: research advances and new challenges. *National science review* 7, 1856-1858, 2020.
- [14] Mamur, Hayati, M. R. A. Bhuiyan, Fatih Korkmaz, and Mustafa Nil. A review on bismuth telluride (Bi<sub>2</sub>Te<sub>3</sub>) nanostructure for thermoelectric applications. *Renewable and Sustainable Energy Reviews* 82, 4159-4169, 2018.
- [15] Xu, Bin, Jing Zhang, Gongqi Yu, Shanshan Ma, Yusheng Wang, and Yuanxu Wang. Thermoelectric properties of monolayer Sb<sub>2</sub>Te<sub>3</sub>. *Journal of Applied Physics* 124, 113-165, 2018.
- [16] Wang, Jiangjing, Chongjian Zhou, Yuan Yu, Yuxing Zhou, Lu Lu, Bangzhi Ge and Yudong Cheng Enhancing thermoelectric performance of Sb<sub>2</sub>Te<sub>3</sub> through swapped bilayer defects. *Nano Energy* 79, 465-484, 2021.
- [17] Sun, Yuxin, Haixu Qin, Chenglong Zhang, Hao Wu, Li Yin, Zihang Liu and Shengwu Guo. Sb<sub>2</sub>Te<sub>3</sub> based alloy with high thermoelectric and mechanical performance for low-temperature energy harvesting. *Nano Energy* 107, 141-176, 2023.
- [18] Xia, Junchao, Yi Huang, Xiao Xu, Yong Yu, Yan Wang, Kaitong Sun, Dasha Mao, Yitao Jiao, Hai-Feng Li, and Jiaqing He. Fine Electron and Phonon Transports Manipulation by Mn Compensation for High Thermoelectric Performance of Sb<sub>2</sub>Te<sub>3</sub> (SnTe) n Materials. *Materials Today Physics*, 101, 26-55, 2023.
- [19] Gayner, Chhatrasal, Luke T. Menezes, Yuriy Natanzon, Yaron Kauffmann, Holger Kleinke, and Yaron Amouyal. Development of Nanostructured Bi<sub>2</sub>Te<sub>3</sub> with High Thermoelectric Performance by Scalable Synthesis and Microstructure Manipulations. *ACS Applied Materials & Interfaces* 15, 13012–13024, 2023.



## Time-Dependent Reliability Analysis for Deflection of a Reinforced Concrete Box Girder Bridge

Abrham Gerbre Tarekegn

School of Civil and Environmental Engineering, Addis Ababa Institute of Technology, Addis Ababa, Ethiopia

✉: [abrham.gebre@aait.edu.et](mailto:abrham.gebre@aait.edu.et), : 0000-0003-0172-2905

Received: 01.04.2023, Revised: 21.06.2023, Accepted: 22.06.2023

### Abstract

Prior to casting of concrete, proper supervision and attention to camber provision in bridge construction are required. It is also critical to use an appropriate quality control manual, pay due attention to reinforcement bar placement, and have a high level of formwork design before construction begins. If these issues are not properly addressed, performance of structures will be affected. In this research, performance of a 40.5m box-girder reinforced concrete bridge which was constructed without having proper camber is studied. As camber was the most important issue of the bridge under investigation, the impact on strength and serviceability requirements is compared to the standard. A dynamic load test with an Arduino type accelerometer is performed to assess the bridge's current condition in relation to the serviceability limit requirement. The deterioration of reinforced concrete (RC) sections due to reinforcement corrosion, creep, and an increase in load intensity, as well as the corresponding statistical distributions are considered to estimate the long-term effect of bridge deflection. Time-variant analysis results showed a linear decrease in deflection reliability indices with the bridge's expected service life of 58 years. After strengthening with steel plates, its service period increased to 85 years.

**Keywords:** Accelerometer, box-girder bridge, dynamic load test, reinforcement corrosion, time-variant analysis

### 1. Introduction

Pre-camber is generally an upward deflection provided to counteract the deflection and stress produced during the life time of the structure. Bridge girders are provided with camber to resist dead load deflections, so appropriate caution should be exercised during construction and is critical [1]. If bridge defects or construction problems exist, bridge's performance will be reduced, and reconstruction of these structures requires additional resources [2].

Bridge structure deflection caused by dead loads, live loads, design errors, construction mistakes, overload, and other factors should be minimized as much as possible, and this should be addressed during design, construction and operation phases. If excessive deflection occurs it leads to a structural failure with serious economic and life losses [3]. This could also be the result of poor formwork design and construction. Therefore, proper design and construction methodology should be followed to achieve adequate cambering; failing to do so will ultimately affect the performance of bridges. In this regard, structural health monitoring (SHM) has become an essential tool for performance assessment of bridges under various conditions [4]. For such an activity, dynamic load test can be conducted to assess the behavior of the bridge. In this case, accelerometers have been extensively used for bridge monitoring by directly measuring force and the corresponding deflections of the bridges are computed analytically [5].

The core objective of this study is to investigate the current condition of Beressa bridge, to ultimately assure its safety and to check the bridge's long-term deflection because surveying data shows that the camber is nearly nil after the formwork has been removed. Furthermore, a field load test was performed to monitor the displacement of an existing bridge using accelerometer sensors. The field tests were taken at two critical locations of the bridge



considering variable vehicular speed (varies from 10km/hr to 50km/hr). The verification is mainly focused to assess whether the deflection requirement of the bridge is exceeded or not. Finally, time-variant reliability analysis for deflection was performed to predict the service life of the bridge. Even if provision of camber is missed during construction, the analysis and test result show that the current condition of the bridge is safe as per strength and serviceability requirements. Considering deterioration of concrete and incremental load intensity, the service period of the bridge is estimated to be 58 years.

## **2. Literature Review**

Deflection is one of the key performance evaluation indicators for bridge structure, and it perfectly reflects the bridge's safety and serviceability condition. As a result, it is essential to evaluate the bridge's serviceability and reliability using deflection data [6]. Camber and deflection that differ from those estimated during design may necessitate changes during construction, resulting in increased costs and longer construction period. Bridges are subjected to environmental and loading conditions during their service life, resulting in a reduction in load carrying capacity [7]. Furthermore, due to uncertainties, deflection and camber requirements for bridges are challenging to predict [1].

During service period of bridges, their serviceability and durability gradually deteriorate due to the influence of various factors, which may even result in affecting safety issues. As a result, in order to provide a scientific basis for structural health diagnosis and maintenance decisions to ensure the safe operation of bridges, the service status of bridges must be evaluated throughout their entire service lives. Material properties, load conditions, geometric characteristics, and steel corrosion, among other things, exhibit significant randomness and have a significant influence on the mechanical properties of bridges [8].

Several controlled live load tests are carried out with trucks with known axle weights and configurations by varying loading positions and truck speed. Using the acceleration signal, the displacement signal is obtained analytically [9]. Selection of bridge displacement tracking methods are frequently made based on the site/bridge to be monitored. Traditional approaches, such as linear variable displacement transducers (LVDTs), can be used in a limited number of cases if a fixed reference is available to measure from. Acceleration is typically an easier method used to measure dynamic response of bridges than displacement, the fundamental issue when attempting to integrate acceleration to recover displacements is the presence of low frequency noise in the acceleration signal [10, 11]. In structural engineering, exceeding a beam's deflection limits implies failure of beams in serviceability. Such failure may result in excessive vibrations of the floor slab or beam caused by a lack of stiffness. However, it should be noted that even after excessive deflection, the beam is usually safe from structural failure due to the design, which has taken appropriate precautions to utilize the ductility of the beam as a primitive sign of impending failure [12].

## **3. Strength Evaluation of an Existing Bridge**

### **3.1. Bridge Data**

Beressa bridge, which is located at 128km from Addis Ababa along the main road to Debre Berhan, is a reinforced concrete box-girder bridge that has a clear span of 40m and a bearing shelf width of 0.50m for the bridge seat. The bridge consists of two decks which has a clear carriageway width of 10m each and a curb walkway width of 1.25m. It has five girders, which

are spaced at 2.4m on centerline of girders. They are 2600mm in depth and have a web width of 300mm. The top deck and bottom slab are 200mm thick. Test results revealed that compressive strength of concrete is ranging from 29.5MPa to 53.50MPa and yield strength of the reinforcing bars are ranging from 460MPa to 525MPa. Fig. 1 shows elevation view of Berresa bridge.



Fig. 1. Elevation of Berresa bridge

### 3.2. Design Review

The design review was carried out for different parts of the bridge. The minimum requirements for girder dimensions are as per the AASHTO and ERA BDM [13, 14]. Furthermore, the number of reinforcing bars provided for flexure and stirrups for shear force are found to be adequate. Overall, the findings of the design review clearly indicate that the girders are safe against both maximum flexural and maximum shear action. Materials used in the construction met the minimum requirement stipulated in the design specification. However, since no camber was provided during construction, the requirement for camber was not checked.

### 3.3. Bridge Load Rating

Load rating is usually performed to assess the capacity of bridges against vehicular loading specified in bridge evaluation manuals [15] and it is computed using Eq. (1) [13, 14, 16]. In the case of rating factor calculation for deflection, ‘ $R_n$ ’ is considered as the deflection limit set in bridge design manuals [16].

$$RF = \frac{\phi R_n - \gamma_{D_i} D_i - \gamma_{D_W} DW}{\gamma_{L_i} (L_i + I)} \quad (1)$$

Here,  $RF$  is the rating factor,  $\phi R_n$  is the nominal resistance,  $\phi$  is a resistance factor,  $D_i$  is the effect of dead loads,  $DW$  is the effect of wearing surface,  $L_i$  is the live-load effect,  $I$  is an impact factor for the live-load effect,  $\gamma_{D_i}$  is the dead load factor,  $\gamma_{L_i}$  is a live load factor and  $\gamma_{D_W}$  is a load factor for wearing surface.

### 3.4. Loading Condition

For the computation of effect of live load, a legal load type 3-3 with 36.4ton given in ERA bridge design manual [14] is used. The critical legal load placement (m) and axle load (kN) used for the assessment is shown in Fig. 2. In Fig. 2, CG is the location of the resultant force.

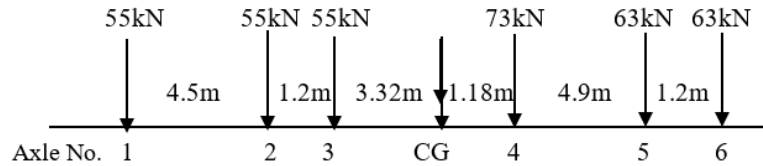


Fig. 2. Truck type 3-3 axle load arrangement

### 3.5. Material Properties

For sectional analysis, compressive strength of concrete for different sections is taken as; 37MPa for top slab, 35MPa for girder web and 29.5MPa for bottom slab. The yield strength of the reinforcing bars is considered as 460MPa.

### 3.6. Load Factors

Load factors are used in structural analysis to determine the design strength and compare it with maximum loads [13]. In this study, for the calculations of rating factors, resistance factor of 0.95 has been used. The load and impact factors used in the assessment are taken from bridge evaluation manuals [13, 14, 16]. As per Table 4.6.2.2.2b-1 and d-1 of AASHTO bridge design specification, the distribution factors for shear and moment are computed as 0.796 and 0.611, respectively and the effects of live loads are multiplied by these factors [16]. The effect of loads of the typical interior girder and the factors are given in Table 1.

Table 1. Effect of loads and different factors

Load Effects	Moment (kN-m)	Shear (kN)	Load Factors	Impact Factors
Dead load	8,420.18	830.59	1.20	-
Live load (legal)	2,780.94	298.58	1.65	1.20
Live load (design)	3,396.05	414.35	1.75	1.33

### 3.7. Section Capacity

Fig. 3 shows the cross section and reinforcement detailing of an interior girder. It has an effective flange width of 2400mm. The capacity of the section is analyzed using Response 2000 software (Reinforced Concrete Sectional Analysis using the Modified Compression Field Theory) and the outputs (bending moment capacity,  $M_{Rd}=26,345\text{kN-m}$  and shear force capacity,  $V_{Rd}=3,464.3\text{kN}$ ) is shown in Fig. 4 (shear force versus shear strain graph is also shown in Fig. 4b) [17].

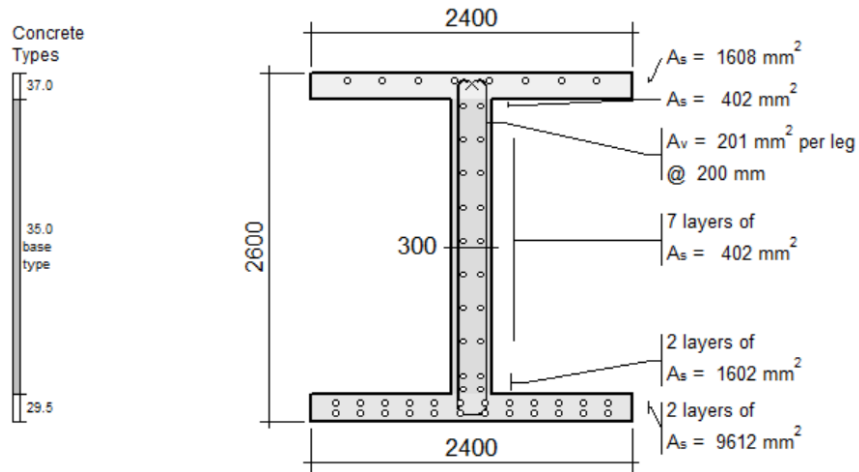


Fig. 3. Cross section of an interior girder

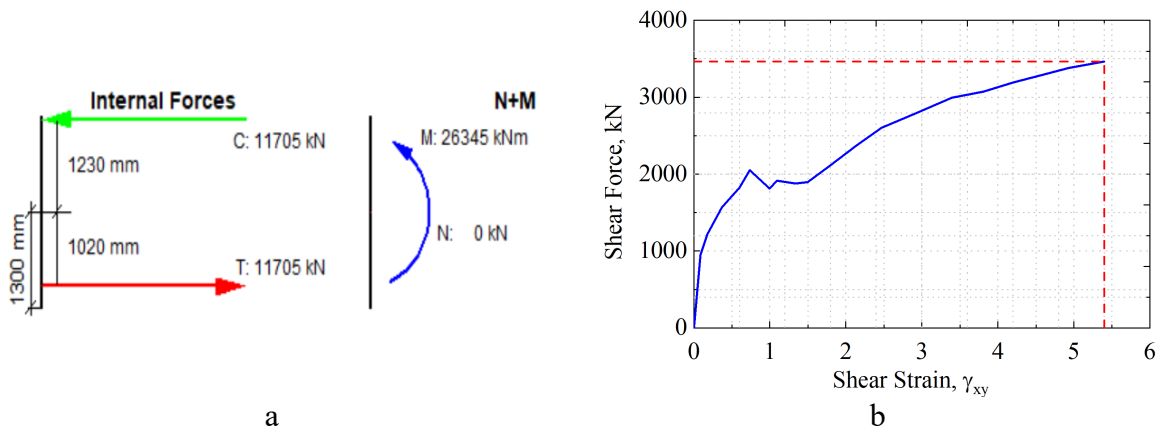


Fig. 4. Capacity of cross section a) bending moment b) shear force

### 3.6. Rating Factor Calculation

The rating factors of the bridge for shear force, bending moment and deflection considering legal truck type 3-3 and design loads are computed deterministically using Eq. (1). The overall deflection of the bridge due to dead and truck type 3-3 load is computed as 35.72mm which is within safe limits,  $L_c/800=50.6\text{mm}$  [14]. The analysis results show that the minimum rating factor of the bridge is computed as 2.90 and 2.94 for legal and design loads, respectively (in both cases, shear force governs). Hence, the bridge is reasonably safe against strength requirements.

The bridge also satisfies serviceability requirements as the rating factors for deflection are 4.85 and 5.38 for design and legal loads, respectively. In this case, Eq. (1) is used with the following conditions;  $R_n$  is the deflection limit (50.6mm),  $D_i$  is deflection due to dead load (31.85),  $L_i$  is the live load deflection (3.86mm and 3.48mm for design and legal loads, respectively). For the computation of live load deflection, distribution factor, impact factor and 25% of the live load (AASHTO Article 3.6.1.3.2) are considered [13].

#### 4. Field Load Test

Load test on bridges is performed to evaluate their load carrying capacities and there are different methods. Among these, dynamic tests are important and are carried out to evaluate dynamic characteristics (natural frequency, mode shape, damping ratio, and so on) [11].

In this study, the field test is designed to assess the performance of the defective girder and solely targeted on the strength, stiffness, and geometry aspects. The equipment and instrumentation used for the field test include; loaded truck-44 ton (loaded with bulk sand) and accelerometer with simulated software. The accelerometer used in this test was an Arduino type accelerometer, MPU-6050.

##### 4.1. Truck Load Test

The wheel arrangement of the truck is measured with a spacing of 3.80m and 1.45m from the front axle to rear ones. The corresponding loads on each of the axles are 11.25ton, 16.875ton and 16.875ton, with a total load of 44tons. The truck used for field load test is shown in Fig. 5.

The truck loading test was mainly aimed to assess the performance of the bridge (stiffness requirement) under moving load action of the loaded truck. The truck weighs 44ton and was made to pass on the bridge at different speeds (10km/hr to 50km/hr). These were considered to assess any potential change in the response of the bridge due to speed or impact. For each loading case, accelerometer measurements were recorded for each position. The sampling frequency for all tests is 10Hz.



Fig. 5. Truck used for loading test - 44ton

##### 4.2. Instrumentation Layout

The actual layout of the bridge showing the locations of accelerometers is shown in Fig. 6. In Table 2, the location of instruments is listed. Critical locations are selected on points of maximum deflection; at interior and exterior girders. The truck loading test was conducted using the set-up presented in Fig. 7.

Table 2. Position of accelerometers

Test No. / Points	x (m)	y (m)	Speed (km/hr)	Remarks
1/A	20.25	1.20	10, 20, 30 and 50	Exterior girder, mid-span
2/B	20.25	1.90	10 and 30	Interior girder, mid-span

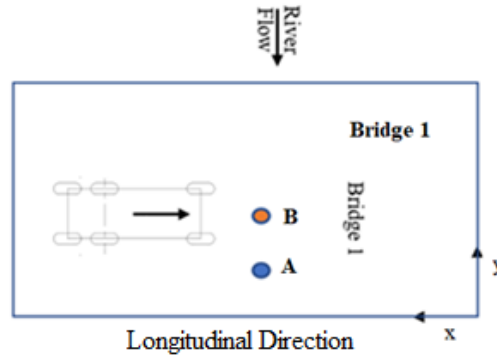


Fig. 6. Position of sensor from plan view of the bridge (not to scale)

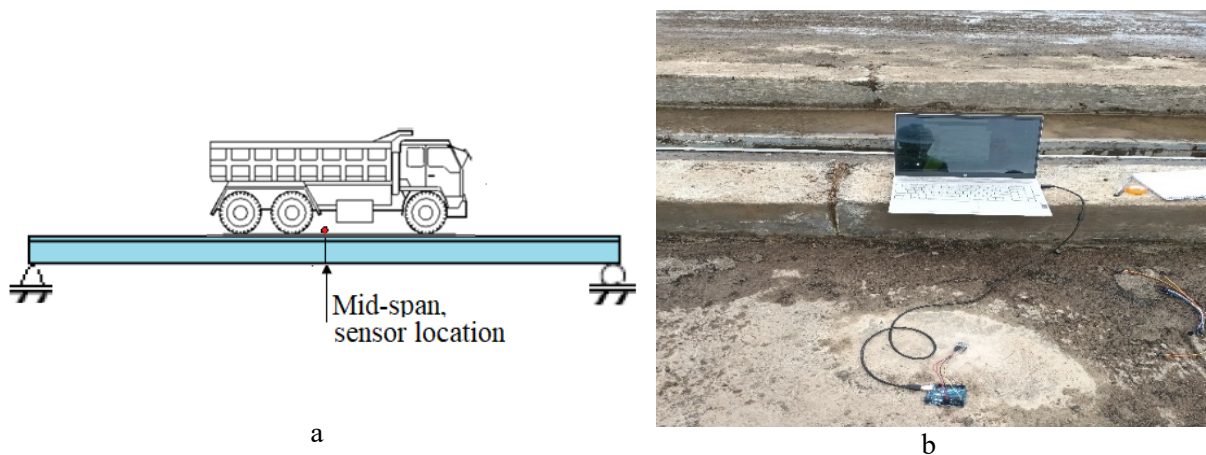
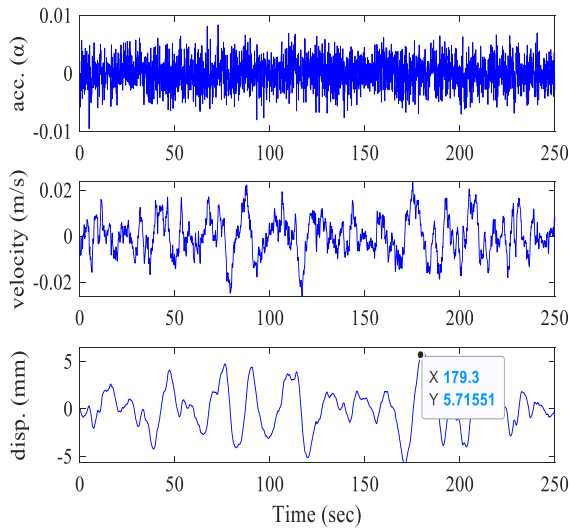


Fig. 7. Set-up for truck loading test and accelerometer

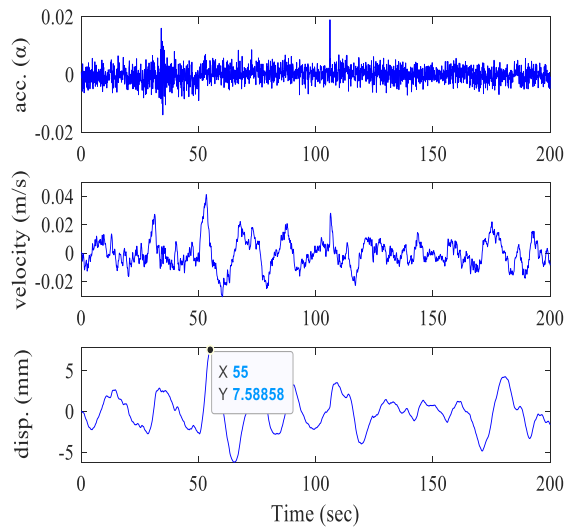
#### 4.4. Truck Loading Test Results

The deflection of the bridge can be calculated by the double integral of the acceleration measured through accelerometers [6]. The recorded acceleration, computed velocity and displacement responses using Fast Fourier Transform (FFT) of the bridge at different locations consisting of a single truck traveling at different speeds are shown in Fig. 8 (a to f). In the figures, the acceleration is expressed in terms of ground acceleration ratio ( $\alpha$ ).

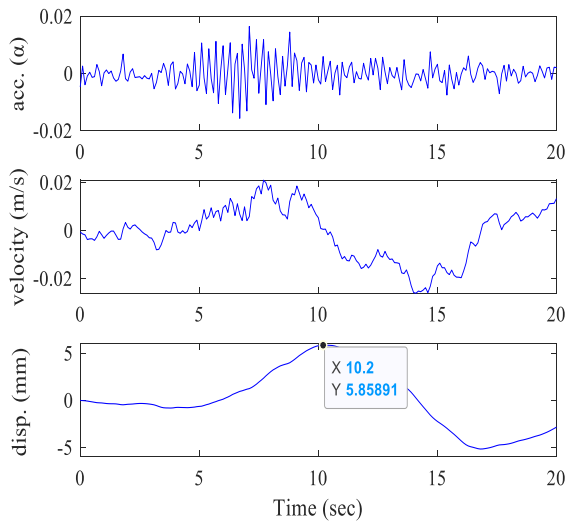
As can be observed from the displacement response curve, the maximum deflection of the bridge is 8.748mm, which occurred at point B with a single truck moving at 30km/hr (Fig. 8f). In contrast, the maximum allowable limit of deflection at mid span is  $L_c/800 = 50.60\text{mm}$  [13]. The actual recorded mid span deflection is one - sixth of the limit for deflection at mid-span, making the girder reasonably safe against serviceability requirements



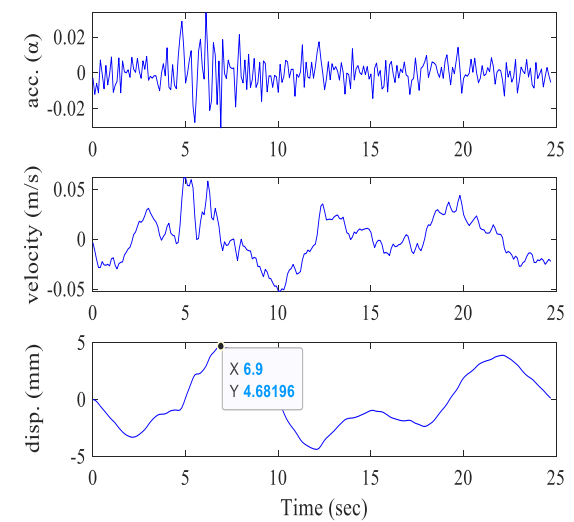
a) Test No. 1, bridge response at 10km/hr



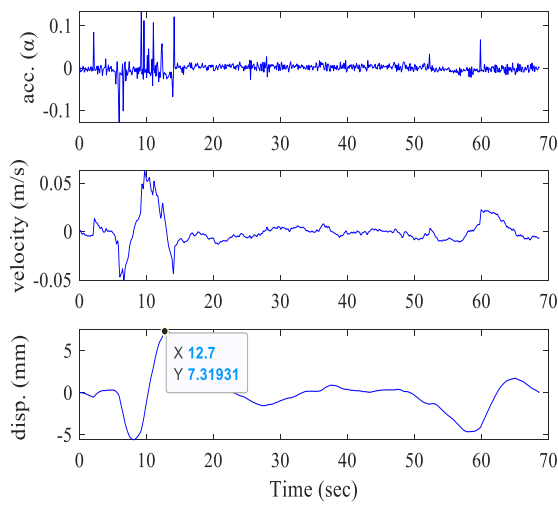
b) Test No. 1, bridge response at 20km/hr



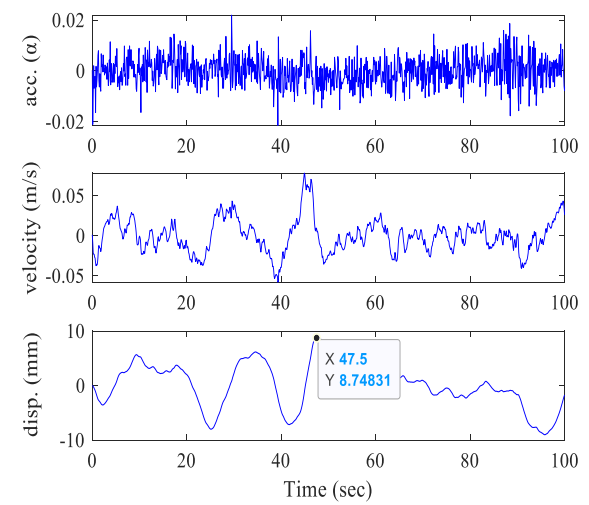
c) Test No. 1, bridge response at 30km/hr



d) Test No. 1, bridge response at 50km/hr



e) Test No. 2, bridge response at 10km/hr



f) Test No. 2, bridge response at 30km/hr

Fig. 8. Bridge responses at critical locations with different vehicular speeds

## 5. Structural Reliability Analysis

### 5.1. Reliability Index

A reliability index is an attempt to quantify a system's reliability using a single numerical value. The requirements to the safety of the structure are consequently expressed in terms of the accepted minimum reliability index ( $\beta$ ) or the accepted maximum failure probability. In a general case, the probability of failure  $P_f$  given in Eq. (2) is defined by the limit state function  $g(x) < 0$  [18] and the limit state function (LSF) is defined in Eq. (2) as the boundary between safety and failure region [15].

$$P_f = P(g(x) < 0)$$

$$g(x) = R(x) - S(x) \quad (2)$$

where  $P_f$  is the probability of failure,  $g(x)$  is the limit state function,  $R(x)$  is the resistance and  $S(x)$  is the load effect. Thus, the first order reliability index is to be computed from Eq. (3) [19]:

$$\beta = \frac{\bar{R} - \bar{S}}{\sqrt{\sigma_R^2 + \sigma_S^2}} \quad (3)$$

where  $\beta$  is reliability index,  $\bar{R}$  and  $\bar{S}$  are mean value of resistance and load effects, respectively.  $\sigma_R$  and  $\sigma_S$  are standard deviations for the resistance and load effects, respectively. For reliability analysis of the bridge under consideration, as shown in Table 3, 12 statistical random variables with five groups have been considered.

Table 3. Statistical distribution of random variables

No.	Random variables	Mean values	CoV (%)	Std. dev.	Distribution
1	Statistical distribution of material properties				
1.1	Yield strength of flexural reinforcement steel (MPa)	436	5	21.80	Lognormal
1.2	Compressive strength of Concrete (MPa)	37	10	3.70	Lognormal
2	Statistical distribution of reinforcement bars				
2.1	Longitudinal bars (mm <sup>2</sup> )	22,507	5	1,125.4	Normal
3	Statistical distribution of force effects				
3.1	Live loads, dead loads, wearing surface	1.00	5	0.05	Normal
3.2	Analysis Variable for DL and LL	1.00	5	0.05	Lognormal
4	Statistical distribution of different factors				
4.1	Resistance factor	0.90	10	0.09	Normal
4.2	Model uncertainty, $N_R$	1.00	4.6	0.046	Lognormal
5	Statistical distribution of bridge dimensions				
5.1	Bridge span (m)	40.5	0.05	0.02	Normal
5.2	Web width (mm)	300	0.5	1.50	Normal
5.3	Web depth (mm)	2600	0.5	13.00	Normal
5.4	Girder spacing (mm)	2400	1.0	24.00	Normal
5.5	Top and bottom slab thicknesses (mm)	200	0.5	1.00	Normal

For reliability assessment of the defective girder, different combinations of random variables of Latin Hypercube Sampling (LHS) are used [20]. In the LHS sampling method, the cumulative distribution function of each factor is divided into intervals with equal probability, and then sampling is done only from each interval [21, 22, 23]. The different combinations of random variables are generated using a MATLAB built-in function for LHS design [24].

As deflection is the major concern of the bridge under consideration, a reliability index for deflection is calculated and compared with the minimum limit. In this scenario, ‘ $R$ ’ is taken as the deflection limit and ‘ $S$ ’ is the deflection of the bridge due to service loads [16]. For the current condition, the probabilistic distributions of  $S$  and  $M$  (design margin= $R-S$ ) for deflection are plotted and shown in Fig. 9. The reliability index for deflection of the bridge is calculated using Eq. (3) and found to be 6.47, i.e.,  $\beta$  is computed by taking the deflection limit as constant ( $\bar{R}=50.6\text{mm}$  and  $\sigma_R=0$ ) and the overall deflection of the bridge (dead and live load deflections) as random variable ( $\bar{S}=35.72\text{mm}$  and  $\sigma_S=2.30$ ). The reliability index of the bridge is within the acceptable standard and exceeds the safety index limit set for newly constructed bridges; which is 3.5 and above [25, 26].

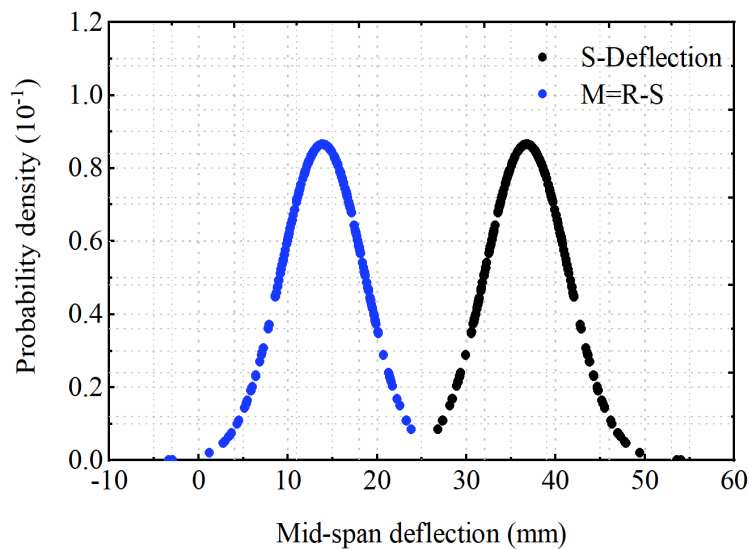


Fig. 9. Probabilistic distribution of S and M for deflection

## 5.2. Time Variant Analysis

As a live load acting on a bridge structure and its resistance changes with time, especially due to deterioration of the structure, the service time of deflection of the bridge (time-dependent deflection) is considered. For time dependent random variables, the limit state function given in Eq. (2) is modified to:

$$P_f = P(g(x(t)) < 0) \quad \text{for } t \in [0, T] \quad (4)$$

In Eq. (4),  $[0, T]$  denotes the reference period, which can be structural life-time or other period of interest. Time-dependent reliability analysis for deflection of the bridge due to dead and live loads are computed to predict service life of the bridge. For time-variant analysis, the followings are considered:

### 5.2.1. Corrosion type

Carbonation-induced corrosion with an exposure class of moderate humidity,  $i_{corr}$  of  $0.10\mu\text{A}/\text{cm}^2$  [27] has been used. Time of corrosion initiation is assumed to be 30 years. The reduction in bar diameter as a function of time assuming uniform corrosion obtained from Eq. (5) is considered [7, 28, 29].

$$\begin{aligned}\phi(t) &= \phi_0 - \alpha P_x(t) \\ P_x(t) &= 0.0116 I_{corr} (t - t_0), t > t_0\end{aligned}\quad (5)$$

Here,  $\phi(t)$  is residual diameter at time  $t$  (mm),  $\phi_0$  is the initial bar diameter (mm),  $a$  is equal to 2 (for carbonated concrete),  $P_x(t)$  is the average value of the attack penetration (decrease of bar radius) at time  $t$ , in mm,  $t_0$  is the time of corrosion initiation (years),  $t$  is elapsed time (years) and  $I_{corr}$  is the corrosion rate ( $\mu\text{A}/\text{cm}^2$ ). As bridge stiffness is deteriorated due to concrete cracking caused by reinforcement corrosion and external load, reinforcement cross-sectional area reduction and bond degradation need to be considered in the analysis. To characterize the influence of various adverse factors caused by reinforcement corrosion on bridge stiffness, the empirical equation given in Eq. (6) can be used [30].

$$I_{ce} = \gamma(\rho) I_e \quad (6)$$

In Eq. (6),  $I_{ce}$  is an effective bending moment of inertia of the bridge after reinforcement corrosion,  $\gamma(\rho)$  is the correction coefficient expressed in Eq. (7) and  $\rho$  is the corrosion rate of reinforcement.

$$\gamma(\rho) = \begin{cases} 1 & \rho \leq 0.05 \\ 1.22 + 12.88\rho^2 - 5.05\rho & \rho > 0.05 \end{cases} \quad (7)$$

### 5.2.2. Time-variant load

In this study, a linear ( $\alpha=1$ ) time-variant load increment given in Eq. (8) is applied for legal truck-type 3-3 with an incremental rate of 0.004 (assuming that over 75 years, the live load intensity increases by 30%) [31].

$$\mu_2(t) = \mu_2(0) \times (1 + at^\alpha) \quad (8)$$

Here,  $\mu_2(t)$  is the load intensity at time  $t$ ,  $\mu_2(0)$  is the initial load intensity,  $\alpha$  is time-variant load increment and  $a$  is the scale factor or annual live load increment (1/year).

### 5.2.3. Creep coefficient

For time-dependent creep coefficient prediction, the creep function given in Eq. (9) is used and the reduced modulus of elasticity of concrete is computed accordingly [32, 33].

$$\varphi(t, t_0) = \frac{(t - t_0)^{0.6}}{10 + (t - t_0)^{0.6}} \varphi(t_0) \gamma_c \quad (9)$$

where,  $\varphi(t, t_0)$  is creep coefficient at time  $t$  due to a load at time  $t_0$ ,  $\varphi(t_0)$  is the ultimate creep coefficient =2.35 [32],  $t$  is age of concrete in days,  $t_0$  is initial time of loading in days and  $\gamma_c$  is creep correction factor for non-standard conditions found in [32].

For time-variant reliability analysis, corrosion rate, load effects, time of corrosion initiation and creep coefficients are considered. Statistical parameters of time-variant random variables with their distributions are shown in Table 4 [20, 25, 34, 35, 36]. Hence, based on the variability of random variables, different combinations have been generated using a MATLAB built-in function for LHS design [24]. Furthermore, the reliability indices of deflection are calculated for 100 years of bridge at various service years at 5-year incremental and the evolution of the reliability indices is obtained.

Table 4. Statistical distribution of time-variant random variables

No.	Random variables	Mean values	CoV (%)	Std. dev.	Remarks
1	Corrosion rate ( $\mu\text{A}/\text{cm}^2$ )	0.10	0.30	0.0003	Lognormal
2	Attach penetration, $P_x(t)$	Eq. (5)	0.02		Lognormal distribution
3	Time variant load effects	Eq. (8)	0.35		Extreme type I
4	Scale factor or load increment ( $a$ )	0.004	0.30	$12 \times 10^{-6}$	Normal distribution
5	Time of corrosion initiation (years)	30	0.20	0.06	Normal distribution
6	Creep coefficient, $\varphi(t_0)$	2.35	10	0.23	Normal distribution

### 5.3. Life Time Prediction and Strengthening

As shown in Fig. 10a, the structural-life of the bridge without the need of any maintenance intervention is predicted as 58 years as the minimal recommended value for evaluation is 2.8 for RC bridges corresponding to a rating factor of 1.0 [25, 33, 37]. After approximately 58 years of service, the reliability index falls below the target value, indicating that the bridge may exhibit greater deflection than expected, necessitating maintenance or speed control actions. Under normal conditions, to carry out maintenance activities, a three-year maintenance plan before the performance of the bridge reaches to the minimum target strength is required [38]. Here,  $t=50$  years is considered as the maintenance intervention period for the Berresa bridge. If strengthening of the reinforced concrete girder bridge using external steel plates (with a thickness of 8mm, overall depth of 1200mm and a steel grade of 235MPa) are proposed as shown in Fig. 10b, the reliability index curve for deflection will be improved and the predicted service period of the bridge will be extended to 85 years, as shown in Fig. 10a. The stiffness of the girder is computed considering the attached steel plates that reduce deflection [39, 40] and reliability indices for deflection are computed accordingly.

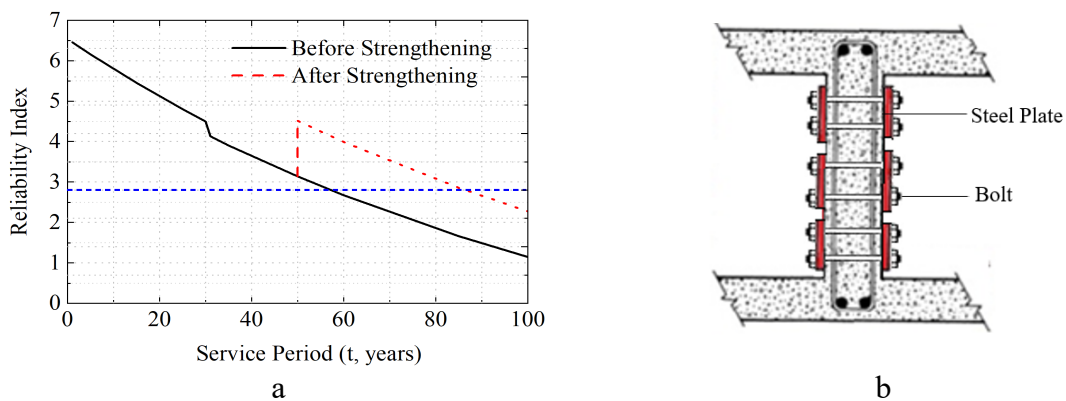


Fig. 10. a) Time-dependent reliability index for 100 years b) cross section of the proposed strengthening method for longitudinal girders

## 6. Conclusions

The performance of the bridge is evaluated through various approaches including design check, strength evaluation through design loads, legal loads and field loading test. The current performance of the bridge satisfies both strength and service limit requirements owing to the fact that the corresponding rating factor and reliability index limits are fulfilled. The numerical and field test results revealed that even if camber was not provided, the bridge is safe from structural failure because of the Strength I design requirements stipulated in design specifications. Time-dependent reliability analysis result; considering time variant loads, possible future reinforcement corrosion and creep effects, shows that the service time of the bridge is predicted as 58 years. The service period of the bridge extended to 85 years if steel plates are attached to longitudinal girders at  $t=50$  years. To ensure the bond between RC girders and external steel plates, mechanical technique of shear connection is required. Regular inspection accomplished with truck load test and strength evaluation is recommended before maintenance intervention is made for strengthening.

## References

- [1] Cakmak, F., Menkulasi, F., Eamon, C. D., Victor, A., and Darwish, I., Evaluation of Camber and Deflections for Bridge Girders; *Michigan Department of Transportation, Research Administration*, 2021.
- [2] ERA: *Standard Specification for Bridge Repair*, Ethiopian Roads Authority, Addis Ababa, 2008.
- [3] Zhang, G., Liu, Y., Liu, J., Lan, S., Yang, J., Causes and Statistical Characteristics of Bridge Failures: A review. *Journal of Traffic and Transportation Engineering (English ed.)*, 9(3), 388-406, 2022.
- [4] Kaloop, M.R., Elbeltagi, E., Hu, J.W., Estimating the Dynamic Behavior of Highway Steel Plate Girder Bridges Using Real-Time Strain Measurements. *Applied Sciences*, 10, 1-16, 2020.
- [5] Meng, X., Roberts, G.W., Cosser, E., Dodson, A.H., Barnes, J. and Rizos, C., Real-Time Bridge Deflection and Vibration Monitoring Using an Integrated GPS/Accelerometer/Pseudolite System, *Proceedings, 11<sup>th</sup> FIG Symposium on Deformation Measurements*, Santorini, Greece, 2003.
- [6] Liu, H., He, X., Jiao, Y., Wang, X., Reliability Assessment of Deflection; Limit State of a Simply Supported Bridge using Vibration Data and Dynamic Bayesian Network Inference. *Sensors*, 19(4), 1-29, 2019.
- [7] Chehade, F.E.H., Younes, R., Mroueh, H., Chehade, F.H., Time-Dependent Reliability Analysis of Reinforced-Concrete Bridges Under the Combined Effect of Corrosion, Creep and Shrinkage. *Safety and Security Environment*, 174, 13-24, 2018.
- [8] Chen, Z., Guo, T., Liu, S., Lin, W., Random Field-Based Time-Dependent Reliability Analyses of a PSC Box-Girder Bridge. *Applied Sciences*, 9(20), 1-20, 2019.
- [9] Vaccaro, R.J., Gindy, M., Nassif, H. and Velde, J., An Algorithm for Estimating Bridge Deflection from Accelerometer Measurements, *Fortieth Asilomar Conference on Signals, Systems and Computers*, IEEE, 2006.

- [10] Bunce, A., Hester, D., Taylor, S., Brownjohn, J., Xu, Y., Case Study: Calculating Bridge Displacement from Accelerations for Load Assessment Calculations. *Civil Engineering Research in Ireland*, 34-39, 2020.
- [11] Ki-Tae, P., Sang-Hyo, K., Heung-Suk, P., Kyu-Wan, L., The Determination of Bridge Displacement using Measured Acceleration. *Engineering Structures*, 27, 371–378, 2005.
- [12] Retrieved from <https://www.quora.com/In-structural-engineering-what-would-happen-if-a-beam-deflected-beyond-its-limits>.
- [13] AASHTO: American Association of State Highway and Transportation Officials, *LRFD Bridge Design Specifications*, 4<sup>th</sup> edition, 2007.
- [14] ERA: *Bridge Design Manual*, Ethiopian Roads Authority, Addis Ababa, 2013.
- [15] Jamali, S., Chan, T.H., Nguyen, A., Thambiratnam, D.P., Reliability-Based Load Carrying Capacity Assessment of Bridges Using Structural Health Monitoring and Nonlinear Analysis. *Structural Health Monitoring*, 18(1), 20-34, 2019.
- [16] AASHTO: American Association of State Highway and Transportation Officials: *The Manual for Bridge Evaluation*, 4<sup>th</sup> edition, 2013.
- [17] Bentz, E.C., and Collins, M.P., *Response 2000: User Manual*, 2001.
- [18] Nowak, A.S. and Collins, K.R., *Reliability of Structures*, CRC Press; 2013.
- [19] Frangopol, D.M., Kozy, B.M., Zhu, B. and Sabatino, S., Bridge System Reliability and Reliability based Redundancy Factors: FHWA-HIF-19-093, US Department of Transportation, Federal Highway Administration, 2019.
- [20] Rücker, W., Hille, F. and Rohrman, R., Guideline for the Assessment of Existing Structures, *Final Report-F08a*, 48pp., 2006.
- [21] Tsubaki, T., Ihara, T., Yoshida, M., Statistical Variation and Modeling of Drying Shrinkage of Concrete, *Trans. of the Japan Concrete Institute*, 14, 123-130, 1992.
- [22] Dutta, S. and Gandomi, A.H., Design of Experiments for Uncertainty Quantification based on Polynomial Chaos Expansion Metamodels, *Handbook of Probabilistic Models*, Elsevier Inc.; 2020.
- [23] Stein, M., Large Sample Properties of Simulations using Latin Hypercube Sampling. *Technometrics*, 29, 143-151, 1987.
- [24] MathWorks, *MATLAB Documentation*, The MathWorks, Inc.; 16<sup>th</sup> edition, 2010.
- [25] Imbsen, R., Liu, W., Schamber, R. and Nutt, R., NCHRP Report 292: Strength Evaluation of Existing Reinforced Concrete Bridges, *Transportation Research Board*, 1987.
- [26] Nowak, A.S., NCHRP Report 368: Calibration of LRFD Bridge Design Code, *Transportation Research Board*, 1999.
- [27] Wang, C., *Structural Reliability and Time Dependent Reliability*, Springer; 2021.

- [28] Baingo, D., *A Framework for Stochastic Finite Element Analysis of Reinforced Concrete Beams affected by Reinforcement Corrosion*, (Doctoral dissertation, Université d'Ottawa/University of Ottawa), 2012.
- [29] Fagerlund, G., *CONTECVET: A Validated User Manual of Assessing the Residual Service Life of Concrete Structures*, Lund University; 2001.
- [30] He, X., Tan, G., Chu, W., Wang, W., Kong, Q., Time-Dependent Reliability Assessment Method for RC Simply Supported T-Beam Bridges Based on Lateral Load Distribution Influenced by Reinforcement Corrosion. *Applied Sciences*, 12(14), 1-18, 2022.
- [31] Wang, C., Li, Q., Simplified Method for Time-Dependent Reliability Analysis of Aging Bridges Subjected to Nonstationary Loads. *International Journal of Reliability, Quality and Safety Engineering*, 23(01), 1-14, 2016.
- [32] ACI 209R-92: American Concrete Institute Committee: Prediction of Creep, Shrinkage, and Temperature Effects in Concrete Structures, *Reported by ACI Committee 209*, 1997.
- [33] Guo, T., Liu, T., Li, A., Deflection Reliability Analysis of PSC Box-Girder Bridge Under High-Speed Railway Loads. *Advances in Structural Engineering*, 15 (11), 2001-2011, 2012.
- [34] Bulleit, W.M., Uncertainty in Structural Engineering. *Practice Periodical on Structural Design and Construction*, 13(1), 24-30, 2008.
- [35] ACI 214R-11: American Concrete Institute Committee: Guide to Evaluation of Strength Test Results of Concrete, *Reported by ACI Committee 214*, 2011.
- [36] Jiang, W., Time-dependent Reliability Analysis for out-plane Stability of CFST Arches, *IOP Conference Series: Earth and Environmental Science*, 2020.
- [37] Nowak, A.S., Szerszen, M.M., Structural Reliability as Applied to Highway Bridges. *Progress in Structural Engineering and Materials*, 2(2), 218–224, 2000.
- [38] Ministry of Public Works and Transports, *Action Plan for Bridge Maintenance Cycle*, Road Infrastructure Department, Kingdom of Cambodia, 2017.
- [39] Kim, M.S., Lee, Y.H., Flexural Behavior of Reinforced Concrete Beams Retrofitted with Modularized Steel Plates. *Applied Sciences*, 11(5), 1-17, 2021.
- [40] Alfeehan A.A., Strengthening of R.C. Beams by External Steel Plate using Mechanical Connection Technique. *Journal of Engineering and Development*, 18, 202-215, 2014.



## A Simple Inspection of Arches, Curved Beams, and Shells

Mustafa Şeker<sup>a\*</sup>, Ömer Civallek<sup>b</sup>

<sup>a</sup> Department of Civil Engineering, Faculty of Engineering, Akdeniz University, Antalya, Turkey

<sup>b</sup> Research Center for Interneural Computing University, China Medical University, Taichung, Taiwan

✉: [mustafaseker07@hotmail.com](mailto:mustafaseker07@hotmail.com)<sup>a\*</sup>, [civalek@yahoo.com](mailto:civalek@yahoo.com)<sup>b</sup>, : 0000-0003-4128-8891<sup>a\*</sup>, 0000-0003-1907-9479<sup>b</sup>

Received: 01.04.2023, Revised: 21.06.2023, Accepted: 22.06.2023

### Abstract

Arches, curved beams and shells are important for structures. This article study provides information on arches, curved beams and shells. Arches, curved beams and shells were examined in sections and briefly explained. In fact, there is a lot of information that can be given about arches, curved beams and shells. In this article study, the terms are briefly explained and tried to be expressed by giving examples with shapes. The application of these terms in modern structures in Civil Engineering is quite common.

**Keywords:** Arches, Shells, Curved Beams.

### 1. Introduction

In recent years, many studies have been done on arches, curved beams and shells. In this article, we tried to provide information about arches, curved beams and shells. In Civil Engineering, many scientists have contributed to human history by doing important work on curved beams, arches and shells. Here, scientists have made applications that will make people's lives easier by contributing to human history. Each scientist has benefited from each other and brought these studies to the best place. The benefits of these studies continue to be obtained by obtaining new results. Scientists have done their own studies and have achieved positive results on arches, curved beams and shells. If we are to express what might be important from these studies; Kiselev emphasized the importance of the theory of curved rods and carried out intensive activities on two hinged arches [1]. When considering the three hinged arches, Rabinovich said that the vertical charge measured from the support is proportional to the coordinates of the vertical coordinate of the arch corresponding to the moment of tilt, and made calculations taking into account the elastic center [2]. Brockenbrough and Meritt compared the Shodek three-hinged arches with two hinged and non-hinged arches in terms of stiffness. As a result, he found that the three hinged arches had less stiffness than the other types of arches [3,4]. Maurizi et al., used the equations of tensile and kinetic energy in the case of non-uniform belt to obtain the bending vibration of the belt [5].

Qatu stated that the beams would be curved, and that they would be deep, shallow, open, closed in terms of curvature. He contributed to important studies by identifying the differences between straight and curved beams [6]. Qatu obtained equations by working on light curved beams. Using these equations, he applied on supported beams [7]. Qatu performed vibration analysis using thin and thick theories on laminated curved beams [8]. Tatemichi et al. they have done important work on viscoelastic layer curved sandwich beams [9]. Chidamparam and Leissa; Markus and Nanasi; Laura and Maurizi performed vibration analysis of curved beams and emphasized that the vibration analysis of curved beams is very important for engineering [10-12]. Morgaevsky, Kolesnik, Karnovsky, Flippov worked on the dynamic effect on shells as



moving loads [16-19]. Karnovsky studied the effect of inertial loads on shells [20]. There are many studies on curved beams, arches and shells. The cumulative progress of these studies has been critical on arches, curved beams and shells. In general, the studies on arches, curved beams and shells described above have led to the work done today.

## 2. Arches

Arches are one of the important elements seen in construction applications from the past to the present. Mainly in historical artifact building applications, arches are seen in road structure applications. If we show the sections of the belt on Figure 1 in order to be better expressed;

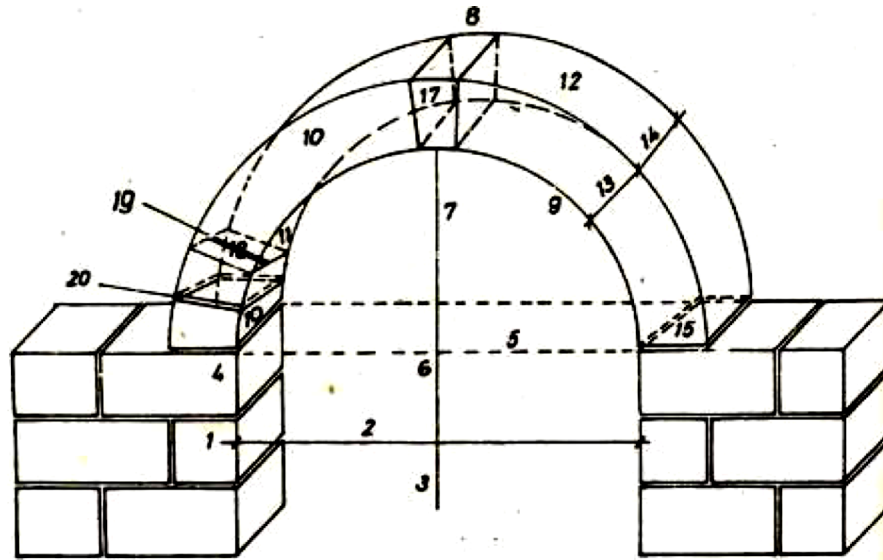


Fig. 1. Sections of the Arches [13]

The number 1 of the sections of the arch shown in Figure 1 are the feet of the arch. The opening of the ground arch expressed by number 2, the ground arch axis expressed by number 3, the ground angle point expressed by number 4, the ground angle level expressed by number 5, the center of the ground arch spring expressed by number 6, the ground arch height expressed by number 7, the floor mount or vertex expressed by number 8, the edge of the arch indicated by number 9, the forehead of the arch indicated by number 10, the abdomen of the arch indicated by number 11, the seat arch indicated by number 12, the thickness of the ground arch expressed by number 13, the width of the ground arch expressed by number 14, the bed of the ground extension expressed by number 15, the floor extension stone expressed by number 16, the place lock stone expressed by number 17, the ground referred to by number 18 is referred to as the arch stones. These sections are very important for the arch [13].

It is possible to see arch applications widely in the countries of the world from the first era to the present. Arch applications are widely seen in Turkey, especially in Ottoman architectures. In the structures where arch applications are seen, it should not be ignored that the structure supports in terms of robustness. This can be seen in some buildings in our country. The fact that they can stand without damage from the moment they are made in the structures supported by arch applications is one of the biggest proofs of this. The arches work in a certain way in the type of structure. The load transfer diagram in a arch is shown as in Figure 2. This diagram describes the exact working principle of the arch.

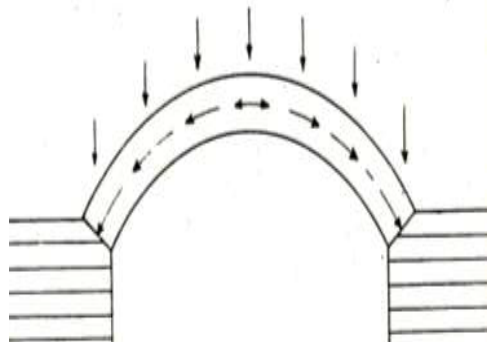


Fig. 2. Load Transfer Diagram in a Arch [13]

Arches are elements of a carrier structure that guide vertical and horizontal loads to specific points. Arches carry the weight they carry with them to the feet. This is why they are reacting to the backlash. The reactions that occur here are generally met with tension irons. But if the iron is corroded or loses its function, it causes damage to the joints. In cases where the tension bars are not used, the belt must be firmly seated on strong walls or the belts must be strengthened with the weight towers [14]. Thus, in Figure 3, an example of a carriage arch in a two-story structure is shown.

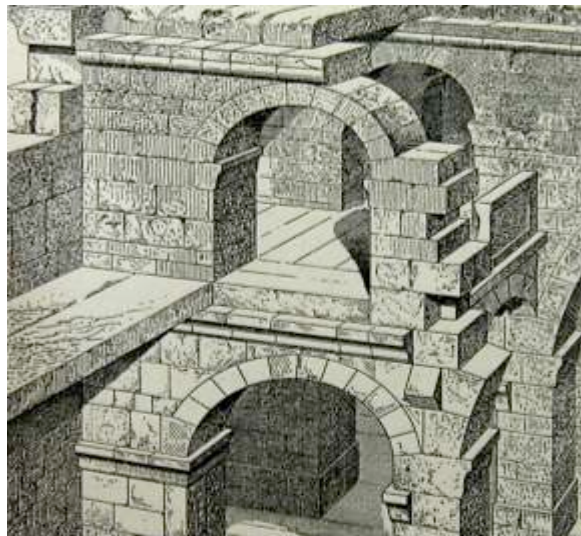


Fig. 3. Carriage Arches in a Two-Story Structure [13]

One of the most important arched structures known to everyone in the world is the Eiffel Tower. The Eiffel Tower was designed by Gustave Eiffel. The general appearance of the Eiffel Tower is shown in Figure 4.



Fig. 4. Overview of the Eiffel Tower [15]

The Eiffel Tower is 300.65 meters high and weighs 7000 tons. Concrete is supported by basic reinforcements. There are approximately 18.000 different parts in this structure; about 2.500.000 rivets, 1.050.846 of which are in place. When this building was built, very skilled human power was used [15].

The Eiffel Tower is located in Paris, the capital of France. This building attracted visitors from many different parts of the world. Even the smallest details in the structure are considered and necessary controls are made both aesthetically and in terms of robustness. It is also possible to see steel construction applications in this structure. Together with the application of steel construction, the structure looks more aesthetically pleasing and at the same time has helped to be more statically sturdy.

There are many examples of structures in the world where arch applications are seen. The number of these buildings is quite large. In the article study, this section briefly gave information about the arches and tried to show them with shapes and the features of the Eiffel Tower, which is one of the most important structures in the world, were shown with the shape. Even in this article study, it was tried to emphasize how important arches are for structures. The sections of the arch are numbered and illustrated in shape and the load transfer principle of the arch is attempted to be illustrated. The features of the arch are briefly explained and the example of the carriage arches in a two-story structure is shown as a figure. Arches come to us in various ways. The most common types of belts; It can be expressed as Low Arch, Pointed Arch, Flat Arch, Horseshoe Arch, Overlap Arch, Kaş Arch, Bursa Arch, Water Arch, Tahfif Arch, Head Arch, Deaf Arch. Pointed Belt application, which is one of these arch types, is shown in Figure 5.

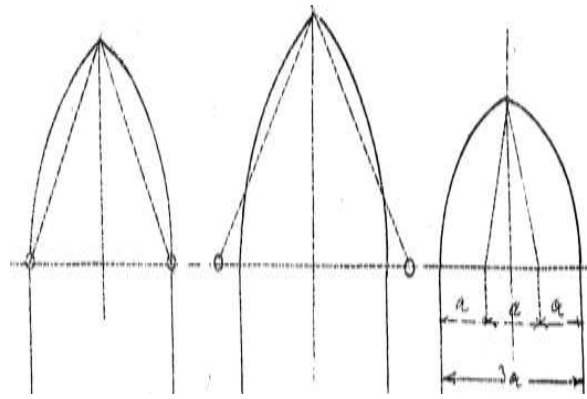


Fig. 5. Pointed Arch Types [13]

### 3. Curved Beams

Laminated composite materials are used to create components such as beams, plates, shells. It is often possible to find laminated beam applications. Beams can be straight or curved. The curved beams feature deep and shallow curvature. Curved beams also have the ability to be open and closed. Here closed beams can be defined as rings and open curved beams. The beams can vibrate at the curvature level and deform. These two features give information about some of the behavior of the beams in the structure and the effect of curvature on the beam vibration. By advancing these studies, scientists have obtained a number of mathematical expressions for straight beams and curved beams. Here the equations for a straight beam are derived by setting the curvature to zero. The radius of curvature that is meant to be described here is to say that it is gone forever [6].

Based on the above, two theories have been obtained for laminated curved beams. In the first theory, thin beams and rotary inertia, in which the effect of cutting deformation is examined, are neglected. This theory is called fine beam theory, or classical beam theory (CBT). To express the second theory, the designed cutting deformation and the rotating inertia effects are explained as follows. This beam theory (SDBT) is called thick beam theory or slip deformation. Figure 6 will show the parameters used for laminated curved beams [6].

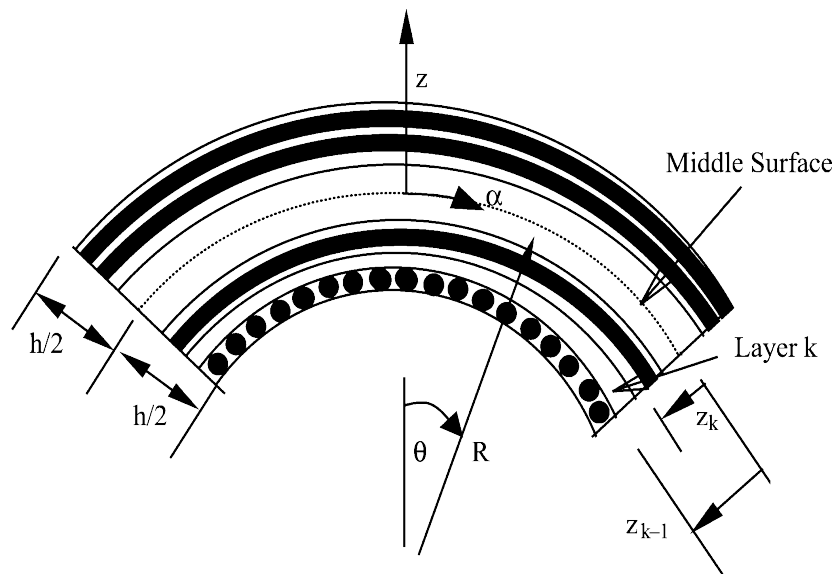


Fig. 6. Parameters Used for Laminated Curved Beams [6]

The basic theory of fine beams is also expressed as the classical beam theory. According to Figure 6, the laminated curved beam is characterized by its mid-surface,  $\alpha$  defined by the polar coordinate. This can be explained mathematically as follows:

$$\alpha = R\theta \tag{1}$$

In Figure 6,  $R$  refers to the radius of curvature of the beam. Equation (1) has been made more special for curved beams. From here, equations for kinematic relations, equations for force and moment results, equations for motion, energy functions and boundary conditions can be obtained. It is important for in-plane loading and vibration in the  $\alpha-z$  plane [6].

The basic theory of medium-thickness beams will be obtained by developing thick beam theory (SDBT) to make thick beams more perfect. The equations obtained for the medium-thickness beam differ from the equations obtained from thin beams. In this theory, by including deformation and rotary inertia, equations for force and moment results, equations for motion equations, energy functions and boundary conditions can be obtained. An accurate mathematical expression can be obtained by incorporating the term  $z/R$  for the stress results of thick beams [6].

The theory of thin beams, using the theories of thick beams, can be obtained mathematical expressions for joists and closed rings that are simply supported. Here, when these equations are obtained, a number of solutions are made by taking into account the boundary condition. In the course of these studies, vibration analysis of fine beams and vibration analysis of thick beams were taken into account. From here, thin beams, medium-thickness beams, closed rings, a number of mathematical equations for numerical results are obtained. In this case, no definite solutions were found.

#### 4. Shells

Shells are defined as a curved surface of a small thickness compared to the size of a structure. The shells carry their own weight, the loads coming from the outside and the loads coming in various forms. The principle of carrying the shell is very different according to the arch. While the amount of thickness is important in the arches, local compression sprain is important in the shells. The wall dome, which is one of the species found in shells, can be seen pressure stretches at very low scales. Figure 7 shows an example of a hemisphere shell. Here it is seen that support is carried out with a proper pressure tension on the shell floor [21].

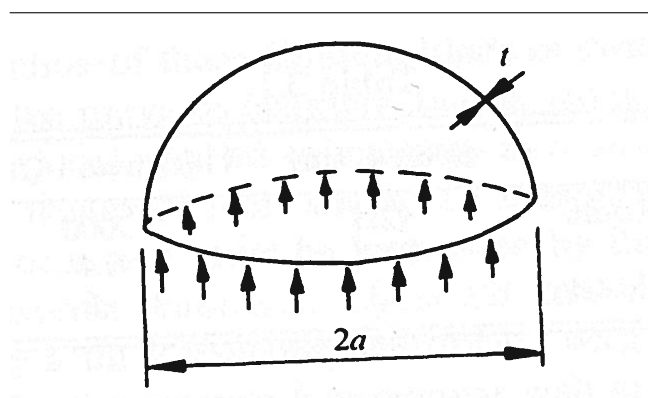


Fig. 7. Half Globe Shell under Its Own Weight Example [22]

Based on the above information, one of the most important methods of dome analysis is that if we express the membrane theory, the ground is weak against bends, therefore the forces cause complete stresses or compressions in the shell [22-32].

Stretches from the shell to the ground analyze the theory transmission. Here, using mathematical equations, Figure 8 and Figure 9 show that elements that occur as a result of stresses in the dome of an element cut from a small shell can be found [21].

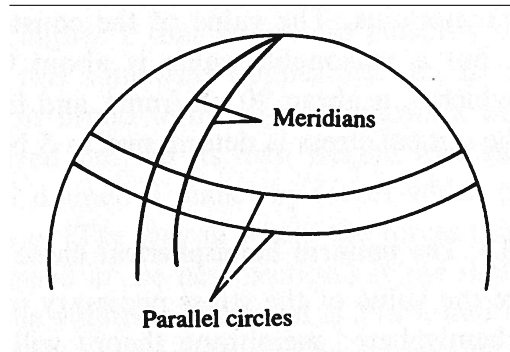


Fig. 8. Defining an Element of the Shell as Meridians and Parallels [22]

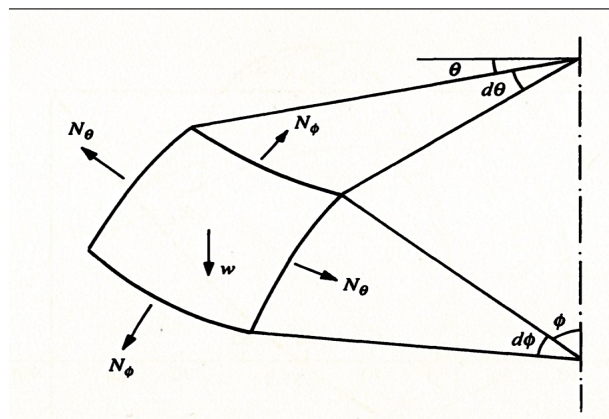


Fig. 9. Balance of a Small Shell Element [22]

Figure 10 illustrates the working principle of a semi-spherical shell balance system [22].

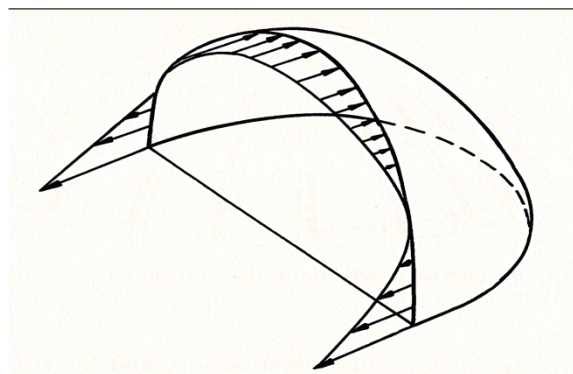


Fig. 10. A Semi-Spherical Shell Balance System [22]

Above, as much as possible, the principles of operation of shells are tried to be explained. Using these working principles, shell applications in modern structures have emerged. The shell applications in these modern structures have supported the robustness of the buildings. The external appearance of these applications looks aesthetically beautiful. Examples of modern structures can be seen predominantly in European countries. One of the modern shell applications in Europe is shown in Figure 11. The name of the structure shown in Figure 11 is the roof of the Zarzuela Hippodrome. The roof was designed by Eduardo Torroja.

Construction of the Zarzuela Hippodrome began in 1935. By making architectural aesthetics and the most appropriate structural solution, this structure took the form of a flat roof as simple as obtaining a hyperboloid. Here, it was seen that the thickness of the reinforced concrete shell changed by 65 cm. After this construction was completed, a modern structure emerged [15].



Fig. 11. Zarzuela Hippodrome by Eduardo Torroja [15]

## 5. Conclusions

Extensive work has been done on arches, curved beams and shells. In this article study, the sections of the arches were expressed in numbers and tried to be explained one by one. Then the exact working principle of the belt was expressed by showing the form. Examples of the arch structures are given and the characteristics of the Eiffel Tower are explained and shown with the shape. By expressing the types of arches, pointed arches, which is one of them, are shown in the figure. Curved beams are mentioned in this article. Two theories are mentioned for curved beams. Thin beam theory and Thick beam theory are explained. The parameters used for curved beams are shown in the figure. Finally, in this article, the shells are mentioned and the hemispherical shell example, the definition of one element of the shell as meridians, the balance of a small shell element and a hemispherical crustal balance system are shown in the figure. As an example of modern shell application, the Zarzuela Hippodrome is illustrated and its features are explained. In this article, it has been tried to be explained with examples by referring to arches, curved beams and shells. As a result, this article study was made with the thought that it would be useful for applications in Civil Engineering.

## References

- [1] Kiselev, V.A., Киселев В.А., Строительная механика. М., Стройиздат, 1960.
- [2] Rabinovich, I.M., Рабинович И.М., Основы строительной механики стержневых систем, 3 изд. М., Госстройиздат, 1960.
- [3] Brockenbrough, R.L., Merritt, F.S., Structural Steel Engineers' Handbook, 4th ed. McGraw-Hill, New York, 2006.
- [4] Schodek, D.L., Structures, 5th ed., Pearson Education, New Jersey, 1980.
- [5] Maurizi, M.J., Rossi, R.E., Belles, P.M., Lowest natural frequency of clamped circular arcs of linearly tapered width., *Journal of Sound and Vibration*, 144(2), 1990.
- [6] Qatu, M.S., Vibration of Laminated Shells and Plates, Amsterdam, The Netherlands, Elsevier Academic Press, 75-105, 2004.
- [7] Qatu, M.S., Inplane vibration of slightly curved laminated composite beams, *Journal of Sound and Vibration*, 159, 327–338, 1992.
- [8] Qatu, M.S., Theories and analyses of thin and moderately thick laminated composite curved beams, *The International Journal of Solids and Structures*., 30(20), 2743–2756, 1993.
- [9] Tatemichi, A., Okazaki, A., Hikyama, M., Damping properties of curved sandwich beams with viscoelastic layer, *Bulletin of the Nagoya Institute of Technology*, 29, 309–317, 1980.
- [10] Chidamparam, P., Leissa, A.W., Vibrations of planar curved beams, rings and arches, *Applied Mechanics Reviews*, 46(9), 467–482, 1993.
- [11] Markus, S., Nanasi, T., Vibrations of curved beams, *The Shock and Vibration Digest*, 7(4), 3-14, 1981.
- [12] Laura, P.A.A., Maurizi, J.A., Recent research on vibrations of arch-type structures, *The Shock and Vibration Digest*, 19(1), 6–9, 1987.
- [13] Milli Eğitim Bakanlığı, Taşın Mimaride Kullanımı, İnşaat Teknolojisi. Ankara, 20-26, 2013.
- [14] Çakır F., Özkal F.M., Uysal H., Sonlu Elemanlar Yöntemi ile Farklı Yükleme Durumları Altındaki Yığma Kemerlerin Yapısal Başarımlarının İncelenmesi, *Tarihi Eserlerin Güçlendirilmesi ve Geleceğe Güvenle Devredilmesi Sempozyumu*, 215-226(1), Erzurum, 1-3 Ekim 2015.
- [15] Roca, P., Laurenço, P.B., Gaetani, A., Historic Construction and Conservation Materials, Systems and Damage, Routledge, New York, 324, 2019.
- [16] Morgaevsky, A.B., Моргаевский АБ. Колебания, статическая и динамическая устойчивость арок. Дисс. на соиск.уч. степ. докт. техн. наук. М., МИСИ, 1961.
- [17] Kolesnik, I.A., Колесник ИА., Колебания комбинированных арочных систем под действием подвижных нагрузок, Киев, Вища школа, 1977.

- [18] Karnovsky, I.A., Карновский, И.А., Колебания пластин и оболочек несущих подвижную нагрузку, Автореф, дисс. на соиск.уч, степ. канд.техн. наук, Дн-ск, Инж-строит, институт, 1970.
- [19] Filippov, A.P., Филиппов АП, Колебания деформируемых систем, М., Машиностроение, 1970.
- [20] Karnovsky, I.A., Карновский И.А., Оптимальная виброзащита деформируемых элементов конструкций, машин и приборов, Автореф.дисс, на соиск.уч, степ. докт. техн. наук, Тбилиси: Груз. политехн. институт, 1989.
- [21] Georg, R., Historical Analysis of Arches and Modern Shells, in Degree of Master of Science, Faculty of the Graduate School of the University of Colorado, Boulder, Colorado, USA, 166, 2014.
- [22] Heyman, J., The Stone Skeleton: Structural Engineering of Masonry Architecture, Cambridge University Press, 1997.
- [23] Numanoglu, H.M., Ersoy, H., Akgöz, B., Civalek, Ö., A new eigenvalue problem solver for thermo-mechanical vibration of Timoshenko nanobeams by an innovative nonlocal finite element method, *Mathematical Methods in the Applied Sciences*, 45(5), 2592-2614, 2022.
- [24] Jalaei, M.H., Thai, H.T., Civalek, Ö., On viscoelastic transient response of magnetically imperfect functionally graded nanobeams, *International Journal of Engineering Science*, 172, 103629, 2022.
- [25] Demir, C., Mercan, K., Numanoglu, H.M., Civalek, O., Bending response of nanobeams resting on elastic foundation, *Journal of Applied and Computational Mechanics*, 4(2), 105-114, 2018.
- [26] Akbaş, Ş.D., Ersoy, H., Akgöz, B., Civalek, Ö., Dynamic analysis of a fiber-reinforced composite beam under a moving load by the Ritz method, *Mathematics*, 9(9), 1048, 2021.
- [27] Esmaeili, H.R., Kiani, Y., Beni, Y.T., Vibration characteristics of composite doubly curved shells reinforced with graphene platelets with arbitrary edge supports, *Acta Mechanica*, 233(2), 665-683, 2022.
- [28] Civalek, Ö., Akbaş, Ş. D., Akgöz, B., & Dastjerdi, S., Forced vibration analysis of composite beams reinforced by carbon nanotubes, *Nanomaterials*, 11(3), 571, 2021.
- [29] Mercan, K., Numanoglu, H. M., Akgöz, B. Demir, C., Civalek, Ö. Higher-order continuum theories for buckling response of silicon carbide nanowires (SiCNWs) on elastic matrix, *Archive of Applied Mechanics*, 87, 1797-1814, 2017.
- [30] Akgöz, B., Civalek, Ö., Investigation of size effects on static response of single-walled carbon nanotubes based on strain gradient elasticity, *International Journal of Computational Methods*, 9(2), 1240032, 2012.
- [31] Petyt, M., Fleischer, C. C., Free vibration of a curved beam, *Journal of Sound and Vibration*, 18(1), 17-30, 1971.

- [32] Dastjerdi, S., Akgöz, B., Civalek, Ö., Malikan, M., Eremeyev, V. A., On the non-linear dynamics of torus-shaped and cylindrical shell structures, *International Journal of Engineering Science*, 156, 103371, 2020.